Time resolution of silicon pixel sensors

W. Riegler, G. Aglieri Rinella

CERN EP, CH-1211 Geneve 23

Abstract

We derive expressions for the time resolution of silicon detectors, using the Landau theory as a minimum model for describing the charge deposit of high energy particles. First we use the center of gravity time of the induced signal and derive analytic expressions for the three components contributing to the time resolution, namely charge deposit fluctuations, noise and fluctuations of the signal shape due to weighting field variations. Then we derive expressions for the time resolution using leading edge discrimination of the signal for various shaping times. Some aspects of time resolution for silicon detectors with gain are discussed as well.

Keywords: silicon sensors, time resolution, weighting field, silicon pixels
PACS 29.40.Cs, 29.40.Gx, 6.30.Ft

1. Introduction

Silicon pixel sensors providing precise timing are currently being developed in view of future "4D" tracking applications. The NA62 Gigatracker, using sensors of $200\,\mu$m thickness and $300\,\mu\text{m}\times300\,\mu$m pixel size has achived time resolutions of ≤ 150 ps at rates of up to $1.5\,\text{MHz/cm}^2$ [1][2][3][4]. A time resolution of 100 ps has been reported with a sensor of $100\,\mu$m thickness and $800\,\mu\text{m}\times800\,\mu$m pixel size [5]. With the introduction of internal amplification inside silicon detectors of $50\,\mu$m thickness, the so called Low Gain Avalanche Diode (LGAD) [6][7][8][9][10], time resolutions of 25 ps have been achieved [11]. The Weightfield2 program [12] allows the detailed simulation of the induced signals in silicon sensors with strip geometry. A long term goal of these developments are pixel sensors of $10\,\mu$m position resolution and 10 ps time resolution [13][14]. Developments of silicon sensors for increased timing performance based on 3D sensors are also described in literature [15]. Studies of front-end electronics for silicon detectors with emphasis on timing aspects can be found in [16] and [17]. Charged particle imaging is widely employed in many areas of science beyond high energy physics, for example as part of material analysis techniques. Therefore there is a broad interest in the developments of spatially resolved and time accurate particle detectors [18][19].

In this report we derive analytic expressions for the time resolution of silicon sensors using the Landau theory as a minimum model describing the charge deposit of high energy particles. We first investigate the time resolution for the case where we take the 'center of gravity time' of the signal as a measure of time. It refers to the case where the amplifier peaking time is larger than the drift time of the electrons and holes in the silicon sensor and allows us to discuss the achievable time resolution using moderate electronics bandwidth together with optimum filter methods to extract the time information from the known signal shape. We then derive formulas quantifying the effect of signal fluctuations due to the finite pixel size and related variations of the weighting field. Finally we derive expressions for the time resolution using leading edge discrimination of the signals with different amplifier integration times.

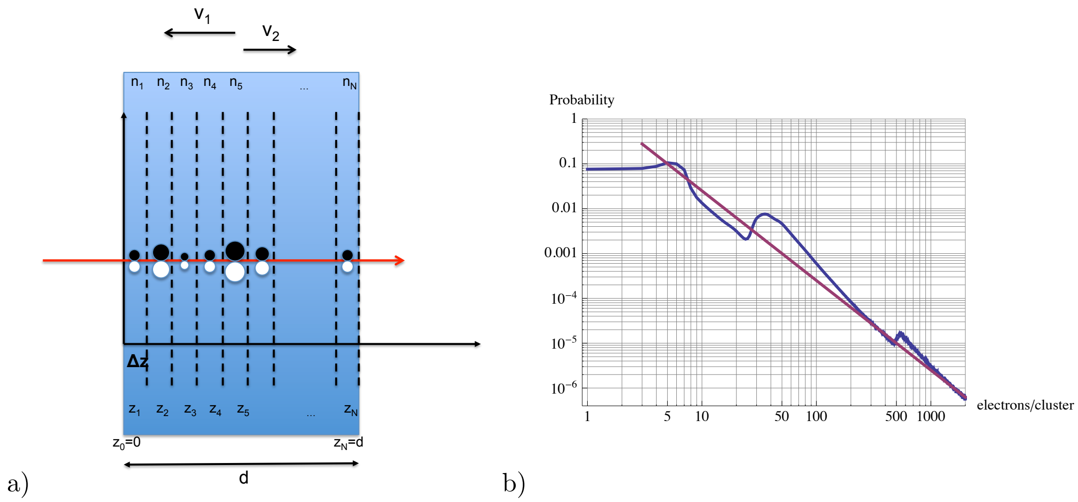

Figure 1: a) The silicon sensor is divided into slices of thickness Δz. The electrons and holes produced in one slice are assumed to move to the boundary of the sensor at constant velocity, which is correct in the limit of negligible depletion voltage. b) Probability to find n electrons per primary interaction. The straight line refers to the $1/n^2$ distribution that is the basis for the Landau distribution, the other curve corresponds to a PAI model [21].

2. Energy deposit

A high energy particle passing a silicon sensor will experience a number of primary interactions with the material, with λ being the average distance between these primary interactions. For relativistic particles we have $\lambda \approx 0.25\,\mu$m in silicon [20]. The electrons created in these primary interactions will typically lose their energy over very small distances and create a localised cluster of electron-hole pairs. We call the probability $p_{cl}(n)$ for creating n e-h pairs in a primary interaction the 'cluster-size distribution'. Throughout this report we treat n as a continuous variable. We now divide the silicon sensor of thickness d into N slices if thickness $\Delta z = d/N$ as shown in Fig. 1a. In case $\Delta z \ll \lambda$, the probability of having zero interactions in Δz is $1 - \Delta z/\lambda$, the probability to have one interaction in Δz is $\Delta z/\lambda$ and the probability to have more than one interaction is negligible, so the probability density for finding n electrons in Δz is

$$p(n, \Delta z)dn = \left(1 - \frac{\Delta z}{\lambda}\right)\delta(n)dn + \frac{\Delta z}{\lambda} p_{clu}(n)dn \tag{1}$$

The probability $p(n, d)$ to have n electrons in the entire thickness d is then given by the N times self convolution of this expression. Since convolution becomes multiplication if we perform the Laplace transform, N times self convoluting the above expression results in raising it's Laplace transform to the power N. So using the Laplace transform $P_{clu}(s) = \mathcal{L}[p_{clu}(n)]$ we have

$$P(s, d) = \mathcal{L}[p(n, d)] = \mathcal{L}[p(n, \Delta z)]^N = \left(1 + \frac{d}{\lambda N}(P_{clu}(s) - 1)\right)^N \tag{2}$$

By taking the limit of $N \to \infty$ we have

$$p(n, d) = \mathcal{L}^{-1}\left[e^{d/\lambda (P_{clu}(s)-1)}\right] \tag{3}$$

The cluster size distribution $p_{clu}(n)$ is typically calculated using some form of the the PAI model [21] and an example is shown in Fig. 1b [20]. For this report we use Landau's approach to assume an $1/E^2$

distribution for the energy transfer in accordance with Rutherford scattering on free electrons and a lower cutoff energy ϵ chosen such that the average energy loss reproduces the Bethe-Bloch theory. The resulting cluster size distribution for a MIP in silicon therefore becomes a $1/n^2$ distribution with a cutoff at $n \approx 2.5$ electrons, according to

$$p_{clu}(n) \approx \frac{2.50}{n^2}\,\Theta(n-2.50) \tag{4}$$

with $\Theta(x)$ being the Heaviside step function. Performing the Laplace transform of this expression and evaluating Eq. 3 results in

$$p(n,d)dn = \frac{\lambda}{2.50\,d}\,L\left(\frac{\lambda}{2.50\,d}\,n + C_\gamma - 1 - \log\frac{d}{\lambda}\right)dn \qquad L(x) = \frac{1}{\pi}\int_0^\infty e^{-t\log t - x\,t}\,\sin(\pi t)dt \tag{5}$$

where $L(x)$ is called the Landau distribution and $C_\gamma = 0.5772...$ is the Euler-Mascheroni constant. The most probable number of e-h pairs n_{MP} and the full width of half maximum n_{FWHM} of $p(n,d)$ are

$$n_{MP} \approx \frac{2.50\,d}{\lambda}\left(0.2 + \log\frac{d}{\lambda}\right) \qquad \frac{\Delta n_{FWHM}}{n_{MP}} \approx \frac{4.02}{0.2 + \log d/\lambda} \tag{6}$$

The most probable number of e-h pairs for a MIP in $50, 100, 200, 300\,\mu$m of silicon evaluate to $\approx 2750, 6190, 13770, 21870$, which is within 10% of the values given in [22]. The relative width $\Delta n_{FWHM}/n_{MP}$ is 0.73, 0.65, 0.58, 0.55 for these values of thickness, which is 20-50% higher than the numbers from the PAI model and the actual values. It is well known that the Landau distribution overestimates the charge deposit fluctuations, so using this model we should have a slightly pessimistic estimate of the time resolution.

3. Center of gravity time of a signal

First we assume the measured time to be defined by the center of gravity (c.o.g.) time of the induced detector current signal $i(t)$. Assuming the Laplace Transform of the signal $I(s) = \mathcal{L}[i(t)]$, the c.o.g. time τ_{cur} of the signal is given by

$$\tau_{cur} = \frac{\int_0^\infty t\,i(t)dt}{\int_0^\infty i(t)dt} = \frac{\int_0^\infty t\,i(t)dt}{q} = -\frac{I'(0)}{I(0)} \tag{7}$$

where $q = \int_0^\infty i(t)dt$ is the total signal charge. We now consider the signal $i(t)$ to be processed by an amplifier having a delta response $f(t)$ with Laplace Transform $F(s)$, so the amplifier output signal $v(t)$ is given by

$$v(t) = \int_0^t f(t-t')i(t')dt' \qquad V(s) = F(s)I(s) \tag{8}$$

The c.o.g. time of the output signal is then given by

$$\tau_v = -\lim_{s\to 0}\frac{V'(s)}{V(s)} = -\frac{F'(0)I(0) + F(0)I'(0)}{F(0)I(0)} = -\frac{F'(0)}{F(0)} - \frac{I'(0)}{I(0)} = \tau_{amp} + \tau_{cur} \tag{9}$$

The represents the sum of the c.o.g. time of the delta response and the one from the current signal, and since the shape of the delta response does not vary in time, the c.o.g. time variation of the of the amplifier output signal is equal to the c.o.g. time variation of the original input signal and has no dependence on the amplifier characteristics.

To determine τ by recording the signal shape and performing the integral of Eq. 7 is not very practical, it is easier to simply process the signal with an amplifier that is 'slow' compared to the signal duration, as shown in the following. In case the duration T of the signal $i(t)$ is short compared to the 'peaking time' t_p of the amplifier ($i(t) = 0$ for $t > T \ll t_p$) we can approximate Eq. 8 for $t > T$ according to

$$\begin{aligned} v(t) &= \int_0^T f(t-t')i(t')dt' \approx \int_0^T \left[f(t) - f'(t)t'\right] i(t')dt' \\ &= q\left[f(t) - f'(t)\frac{\int_0^T t'i(t')dt'}{q}\right] = q\left[f(t) - f'(t)\tau_{cur}\right] \\ &\approx q\, f(t-\tau_{cur}) \end{aligned} \tag{10}$$

The amplifier output is simply equal to the amplifier delta response shifted by the c.o.g. time of the current signal and scaled by the total charge of the signal. Since the shape of the amplifier output signal is always equal to the amplifier delta response, we can determine the signal c.o.g. time either by the threshold crossing time at a given fraction of the signal or by sampling the signal and fitting the known signal shape to the samples.

For later use we remark that for the sum of two current signals $i(t) = i_1(t) + i_2(t)$ with c.o.g. times τ_1 and τ_2 we have

$$\tau = \frac{\int ti(t)dt}{\int i(t)dt} = \frac{\tau_1 \int i_1(t)dt + \tau_2 \int i_2(t)dt}{\int i_1(t)dt + \int i_2(t)dt} = \frac{\tau_1 q_1 + \tau_2 q_2}{q_1 + q_2} \tag{11}$$

The c.o.g. time for the sum of N signals $i_n(t)$ is therefore given by

$$\tau = \frac{1}{\sum_{k=1}^N q_k} \sum_{k=1}^N q_k\, \tau_k \tag{12}$$

4. Variance of the center of gravity time of a silicon detector signal

We assume a silicon sensor operated at large over-depletion i.e. at a voltage that is large compared to the depletion voltage and the electric field can therefore be assumed to be constant throughout the sensor. Consequently the velocities of electrons and holes are constant and the signal from a single electron or single hole has a rectangular shape. We assume a parallel plate geometry with one plate a $z = 0$ and one at $z = d$, where a pair of charges $+q, -q$ is produced at position z and $-q$ moves with velocity v_1 to the electrode at $z = 0$ while q moves with velocity v_2 to the electrode at $z = d$. The weighting field of the electrode at $z = 0$ is $E_w = 1/d$ and the induced current is therefore

$$i(t) = -\frac{qv_1}{d}\Theta(z/v_1 - t) - \frac{qv_2}{d}\Theta((d-z)/v_2 - t) \tag{13}$$

with $\Theta(t)$ being the Heaviside step function. We have $\int i(t)dt = -q$ and according to Eq. 7 the c.o.g. time of this signal is then

$$\tau = \frac{1}{2d}\left[\frac{z^2}{v_1} + \frac{(d-z)^2}{v_2}\right] \tag{14}$$

If $n_1, n_2, ..., n_N$ charges are produced at positions $z_1, z_2, ..., z_N$ and are moving to the electrodes with v_1 and v_2, the resulting c.o.g. time of the signal is

$$\tau(n_1, n_2, ..., n_N) = \frac{1}{2d\left(\sum_{k=1}^N n_k\right)} \sum_{k=1}^N n_k \left[\frac{z_k^2}{v_1} + \frac{(d-z_k)^2}{v_2}\right] \tag{15}$$

We now divide the sensor of thickness d into N slices of $\Delta z = d/N$ as shown in Figure 1. The probability to have n_k e/h pairs in slice k is given by the Landau distribution $p(n_k, \Delta z)$ and if we assume that all these charges are moving from position z_k to the electrodes, we have $z_k = k\,\Delta z$ and we can proceed to calculate the variance Δ_τ^2 of the c.o.g. time of the signal, i.e. the time resolution, according to

$$\Delta_\tau^2 = \overline{\tau^2} - \overline{\tau}^2 \tag{16}$$

with $\overline{\tau}$ and $\overline{\tau^2}$ being the average and the second moment of τ. The average $\overline{\tau}$ is given by

$$\overline{\tau} = \int_0^\infty \int_0^\infty ... \int_0^\infty \tau(n_1, n_2, ..., n_N) p(n_1, \Delta z) p(n_2, \Delta z) ... p(n_N, \Delta z)\, dn_1\, dn_2 ... dn_N \tag{17}$$

Since

$$\int_0^\infty \int_0^\infty ... \int_0^\infty \frac{n_1 + n_2 + ... + n_N}{n_1 + n_2 + ... + n_N} p(n_1, \Delta z) p(n_2, \Delta z) ... p(n_N, \Delta z)\, dn_1\, dn_2 ... dn_N = 1 \tag{18}$$

we have

$$\int_0^\infty \int_0^\infty ... \int_0^\infty \frac{n_k}{n_1 + n_2 + ... + n_N} p(n_1, \Delta z) p(n_2, \Delta z) ... p(n_N, \Delta z)\, dn_1\, dn_2 ... dn_N = \frac{1}{N} \qquad k = 1, 2, ..., N \tag{19}$$

and therefore

$$\overline{\tau} = \frac{1}{2d} \sum_{k=1}^{N} \frac{1}{N} \left[\frac{z_k^2}{v_1} + \frac{(d - z_k)^2}{v_2} \right] \approx \frac{1}{2d^2} \int_0^d \left[\frac{z^2}{v_1} + \frac{(d - z)^2}{v_2} \right] dz = \frac{d}{6} \left(\frac{1}{v_1} + \frac{1}{v_2} \right) \tag{20}$$

which is the expected center of gravity of the two triangular signals form the electrons and the holes. The second moment of the c.o.g. time $\overline{\tau^2}$ is given by

$$\overline{\tau^2} = \int_0^\infty \int_0^\infty ... \int_0^\infty \tau^2(n_1, n_2, ..., n_N) p(n_1, \Delta z) p(n_2, \Delta z) ... p(n_N, \Delta z)\, dn_1\, dn_2 ... dn_N \tag{21}$$

$$\tau^2(n_1, n_2, ..., n_N) = \frac{1}{4d^2 \left(\sum_{k=1}^N n_k\right)^2} \sum_{k=1}^{N} \sum_{r=1}^{N} n_k n_r \left[\frac{z_k^2}{v_1} + \frac{(d - z_k)^2}{v_2} \right] \left[\frac{z_r^2}{v_1} + \frac{(d - z_r)^2}{v_2} \right] \tag{22}$$

We define

$$\begin{aligned} a_N &= \int_0^\infty \int_0^\infty ... \int_0^\infty \frac{n_k\, n_r}{(n_1 + n_2 + ... + n_N)^2} p(n_1, \Delta z) p(n_2, \Delta z) ... p(n_N, \Delta z)\, dn_1\, dn_2 ... dn_N \qquad k \neq r \\ b_N &= \int_0^\infty \int_0^\infty ... \int_0^\infty \frac{n_k^2}{(n_1 + n_2 + ... + n_N)^2} p(n_1, \Delta z) p(n_2, \Delta z) ... p(n_N, \Delta z)\, dn_1\, dn_2 ... dn_N \end{aligned} \tag{23}$$

and since we have

$$\int_0^\infty \int_0^\infty ... \int_0^\infty \frac{(n_1 + n_2 + ... + n_N)^2}{(n_1 + n_2 + ... + n_N)^2} p(n_1, \Delta z) p(n_2, \Delta z) ... p(n_N, \Delta z)\, dn_1\, dn_2 ... dn_N = 1 \tag{24}$$

it holds that

$$N\, b_N + N(N-1) a_N = 1 \quad \rightarrow \quad a_N = \frac{1 - N\, b_N}{N(N-1)} \approx \frac{1}{N^2} - \frac{b_N}{N} \tag{25}$$

The second moment of τ therefore becomes

$$\overline{\tau^2} = \frac{b_N}{4d^2}\sum_{k=1}^{N}\left[\frac{z_k^2}{v_1}+\frac{(d-z_k)^2}{v_2}\right]^2 + \frac{a_N}{4d^2}\sum_{k=1}^{N}\sum_{r\neq k=1}^{N}\left[\frac{z_k^2}{v_1}+\frac{(d-z_k)^2}{v_2}\right]\left[\frac{z_r^2}{v_1}+\frac{(d-z_r)^2}{v_2}\right] \quad (26)$$

$$= \frac{b_N-a_N}{4d^2}\sum_{k=1}^{N}\left[\frac{z_k^2}{v_1}+\frac{(d-z_k)^2}{v_2}\right]^2 + \frac{a_N}{4d^2}\sum_{k=1}^{N}\sum_{r=1}^{N}\left[\frac{z_k^2}{v_1}+\frac{(d-z_k)^2}{v_2}\right]\left[\frac{z_r^2}{v_1}+\frac{(d-z_r)^2}{v_2}\right] \quad (27)$$

$$\approx \frac{b_N}{4d^2}\frac{1}{\Delta z}\int_0^d\left[\frac{z^2}{v_1}+\frac{(d-z)^2}{v_2}\right]^2 dz + \frac{a_N}{4d^2}\frac{1}{(\Delta z)^2}\left(\int_0^d\left[\frac{z^2}{v_1}+\frac{(d-z)^2}{v_2}\right]dz\right)^2 \quad (28)$$

$$= \frac{b_N}{\Delta z}\frac{d^3(3v_1^2+v_1v_2+v_2^2)}{60v_1^2v_2^2} + \frac{a_N}{(\Delta z)^2}\frac{d^4(v_1+v_2)^2}{36v_1^2v_2^2} \quad (29)$$

$$= \frac{b_N}{\Delta z}\frac{d^3(4v_1^2-7v_1v_2+4v_2^2)}{180v_1^2v_2^2} + \frac{d^2(v_1+v_2)^2}{36v_1^2v_2^2} \quad (30)$$

and we have for the variance

$$\Delta_\tau^2 = \overline{\tau^2} - \overline{\tau}^2 = \frac{b_N d}{\Delta z}\frac{d^2(4v_1^2-7v_1v_2+4v_2^2)}{180v_1^2v_2^2} \quad (31)$$

The expression for Δ_τ is symmetric with respect to v_1 and v_2, which reflects the fact that the induced signal on the electrode at $z=0$ is always equal (and opposite in sign) to the signal at the electrode at $z=d$. To evaluate b_N

$$b_N = \int_0^\infty\int_0^\infty ... \left[\int_0^\infty \frac{n_1^2\,p(n_1,\Delta z)}{(n_1+n_2+...+n_N)^2}dn_1\right] p(n_2,\Delta z)...p(n_N,\Delta z)\,dn_2...dn_N \quad (32)$$

we change variables according to $n = n_2+n_3+...+n_N$, i.e. $n_2 = n-n_3-n_4-...-n_N$ and $dn_2 = dn$ and see that the expression outside the brackets becomes equal to the the $N-1$ times self convoluted probability $p(n,\Delta z)$ which is simply $p(n, d-\Delta z) \approx p(n,d)$. Using Eq. 1 for small values of Δz the expression therefore becomes

$$b_N = \int_0^\infty\left[\int_0^\infty \frac{n_1^2\,p(n_1,\Delta z)}{(n_1+n)^2}dn_1\right]p(n,d)dn = \int_0^\infty\left[\frac{\Delta z}{\lambda}\int_0^\infty \frac{n_1^2\,p_{clu}(n_1)}{(n_1+n)^2}dn_1\right]p(n,d)dn \quad (33)$$

Up to this point the expression for b_N is still completely general for any kind of cluster size distributions $p_{clu}(n)$ and resulting $p(n,d)$. Using the Landau theory we use $p_{clu}(n)$ from Eq. 4 and have

$$\int_0^\infty \frac{n_1^2\,p_{clu}(n_1)}{(n_1+n)^2}dn_1 = \int_{2.50}^\infty \frac{2.50}{(n_1+n)^2}dn_1 = \frac{2.50}{n+2.50} \approx \frac{2.50}{n} \quad (34)$$

(for $n \gg 1$) and with Eq. 5 we get

$$b_N \approx 2.50\frac{\Delta z}{\lambda}\int_0^\infty \frac{p(n,d)}{n}dn = \frac{\Delta z}{d}\int_0^\infty \frac{L(z+\gamma-1-\log d/\lambda)}{z}dz \approx \frac{\Delta z}{d}\frac{1}{(1+1.155\,\log d/\lambda)} \quad (35)$$

The last expression is an approximation of better than 1% in the interval $4 < \log d/\lambda < 10$, which corresponds to a range of the silicon sensor thickness of $15 < d < 5000\,\mu$m for a value of $\lambda = 0.25\,\mu$m.

For the standard deviation we therefore finally have

$$\Delta_\tau \approx \frac{d}{\sqrt{1+1.155\,\log d/\lambda}}\sqrt{\frac{4}{180 v_1^2}-\frac{7}{180 v_1 v_2}+\frac{4}{180 v_2^2}} \tag{36}$$

This is the time resolution of a silicon sensor when measuring the c.o.g. time. Neglecting the weak dependence on $\log d/\lambda$, at constant electric field i.e. at constant drift velocity v_1 and v_2, the time resolution scales with d, which represents the trivial fact that the duration of the signal and therefore also Δ_τ scales with d. For a given voltage V, the electric fields in the thinner sensors, and therefore the velocities of electrons and holes are of course larger, so the time resolution improves significantly beyond the $1/d$ scaling for thin sensors.

If we associate v_1 and v_2 with the electron and hole velocity, $T_1 = d/v_1$ and $T_2 = d/v_2$ are the total drift times of electrons and holes, and $T_{12} = d/\sqrt{v_1 v_2}$ is the total drift time assuming the geometric mean of the electron and hole velocity. The expression $1/\sqrt{1+1.155\,\log d/\lambda}$ varies only from 0.37 to 0.33 for d from $50\,\mu$m to $300\,\mu$m for $\lambda = 0.25\,\mu$m, which means that the effect of the Landau fluctuations does not vary significantly in this range of sensor thickness. So by approximating it with the value of 0.35 we have

$$\Delta_\tau \approx \frac{1}{20}\sqrt{T_1^2 - 1.75\,T_{12} + T_2^2} \qquad\qquad 50\,\mu\mathrm{m} < d < 300\,\mu\mathrm{m} \tag{37}$$

To get realistic estimates we use an approximation for the velocity of the electrons and holes from [26]

$$v_e(E) = \frac{\mu_e\,E}{\left[1+\left(\frac{\mu_e\,E}{v_{sat}^e}\right)^{\beta_e}\right]^{1/\beta_e}} \qquad\qquad v_h(E) = \frac{\mu_h\,E}{\left[1+\left(\frac{\mu_h\,E}{v_{sat}^h}\right)^{\beta_h}\right]^{1/\beta_h}} \tag{38}$$

where we chose $\mu_e = 1417\,\mathrm{cm^2/Vs}$, $\mu_h = 471\,\mathrm{cm^2/Vs}$, $\beta_e = 1.109$, $\beta_h = 1.213$ and $v_{sat}^e = 1.07\times10^7$ cm/s and $v_{sat}^h = 0.837\times10^7$ cm/s at 300 K in accordance with the default models in Sentaurus Device [23]. The resulting drift velocity together with the time that the electrons and holes need to traverse the sensor (assuming $V_{dep} = 0$) are given in Fig. 2. For a $50\,\mu$m sensor at 200 V the electrons take 0.6 ns and the holes take 0.8 ns to traverse the sensor, so the total signal duration is < 0.8 ns.

The values for the time resolution according to Eq. 36 are given in Fig. 3. For an applied voltage of 200 V the values are 370, 180, 59, 23 ps for 300, 200, 100, $50\,\mu$m sensors. It should be noted that the Landau theory overestimates the charge deposit fluctuations by 20-30% and the resulting c.o.g. time distribution has significant tails, so this standard deviation should be a conservative estimate of the time resolution.

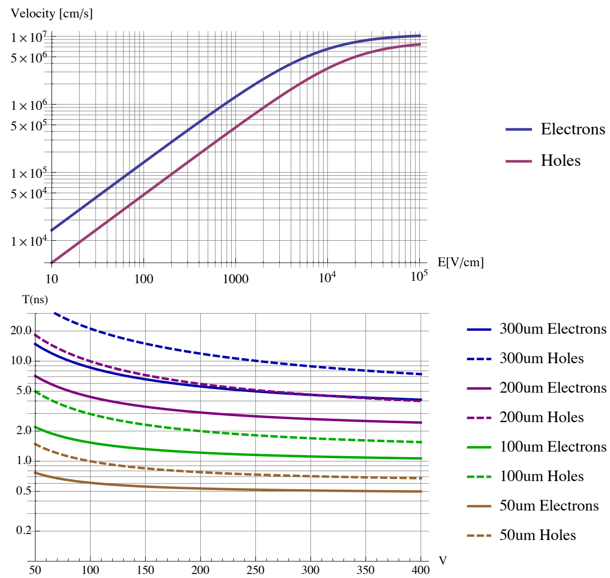

Figure 2: Velocity of electrons and holes as a function of electric field (top) and time for electrons an holes to transit the full thickness of the sensor assuming negligible depletion voltage (bottom).

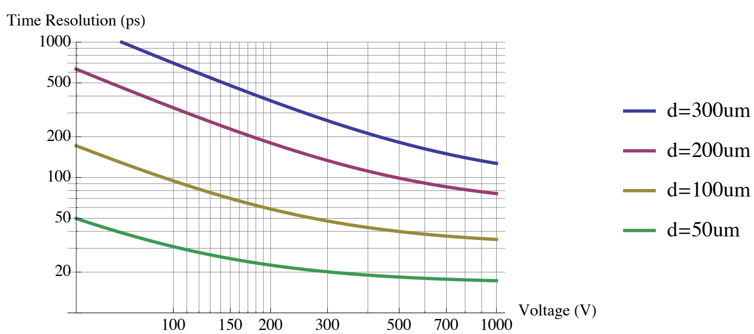

Figure 3: Standard deviation of the c.o.g. time from Eq. 36 for different values of silicon sensor thickness as a function of applied voltage V, assuming $\lambda = 0.25\,\mu$m, the Landau theory and negligible depletion voltage.

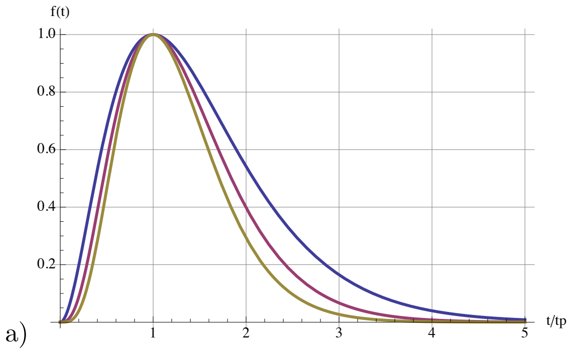

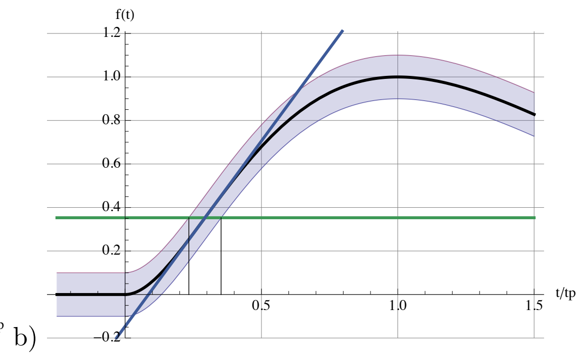

Figure 4: a) Amplifer response for $n = 2, 3, 4$ from Eq. 39. b) Contribution to the time resolution from the noise.

5. Noise contribution to the c.o.g. time

As shown in Eq. 10 the c.o.g. time of a signal can be measured by using an amplifier with a peaking time t_p that is larger than the total signal time T. For a $50\,\mu$m sensor at 250 V this signal time is $T \approx 0.8$ ns, so an amplifier with peaking time $t_p > 1.5$ ns can realise such a measurement. The problem to solve is therefore to measure the time of a pulse with know shape (the delta response) that has noise of a known frequency spectrum superimposed. This can be accomplished by various techniques of constant fraction discrimination or continuous sampling with optimum filtering methods, both of which will be discussed in this section. For the remainder of the report we assume an unipolar amplifier with a delta response of

$$f(t) = \left(\frac{t}{t_p}\right)^n e^{n(1-t/t_p)}\,\Theta(t) \tag{39}$$

where t_p is the peaking time and $\Theta(t)$ is the Heaviside step function. The delta response for $n = 2, 3, 4$ is shown in Fig. 4a. Such an amplifier can be realized by n integration integration stages with $\tau = RC = t_p/n$ and for large values of n it approaches Gaussian shape (semi-gaussian shaping). In general we can use it to parametrize a measured delta response shape by adjusting n and t_p to fit a specific amplifier delta response. The normalized transfer function and related 3 dB bandwidth frequency f_{bw} of the above delta response are given by

$$|W(i2\pi f)| = \frac{1}{\sqrt{[1+(2\pi f)^2 t_p^2/n^2]^{n+1}}} \qquad f_{bw} = \frac{1}{2\pi\, t_p}\, n\sqrt{2^{1/(n+1)}-1} \tag{40}$$

For constant fraction discrimination we set the threshold to a value where $f(t)$ has the maximum slope of $f'(t_s)$ at time t_s which evaluates to

$$t_s = t_p\,(1 - 1/\sqrt{n}) \qquad f'(t_s) = \frac{1}{t_p}\, e^{\sqrt{n}} n^{(3/2-n)} (n-\sqrt{n})^{n-1} \tag{41}$$

Assuming a pulse-height A and a noise of σ_{noise}, the timing error when applying the threshold at the maximum slope is then

$$\sigma_t = \frac{\sigma_{noise}}{A}\,\frac{1}{f'(t_s)} = \frac{\sigma_{noise}}{A}\,\frac{t_p}{e^{\sqrt{n}} n^{(3/2-n)}(n-\sqrt{n})^{n-1}} = \frac{\sigma_{noise}}{A}\,\frac{1}{2\pi f_{bw}}\,\frac{\sqrt{2^{1/(n+1)}-1}}{e^{\sqrt{n}} n^{(1/2-n)}(n-\sqrt{n})^{n-1}} \tag{42}$$

as illustrated in Fig. 4b. This evaluates to

$$
\begin{aligned}
&= \frac{\sigma_{noise}}{A}\; t_p \;\times (0.59, 0.57, 0.54, 0.51) \qquad \text{for} \qquad n = 2, 3, 4, 5 \\
&= \frac{\sigma_{noise}}{A}\frac{1}{f_{bw}} \times (0.10, 0.12, 0.13, 0.14) \qquad \text{for} \qquad n = 2, 3, 4, 5
\end{aligned} \tag{43}
$$

So for an amplifier with a peaking time of t_p=1 ns and $n = 2$, the time resolution is 60 ps for a signal to noise ratio of 10 and 20 ps for a signal to noise ratio of 30.
The pulse-height of the sensor signal is given by the total number n of deposited e-h pairs, so if we write the noise σ_{noise} in units of electrons the signal to noise ratio is σ_{noise}/n. Since n is varying according to the Landau distribution $p(n, d)$ from Eq. 5, using Eq. 35 we can calculate the average signal to noise ratio and the average time resolution to

$$
\overline{\sigma}_t = \frac{\sigma_{noise}}{f'(t_s)} \int_0^\infty \frac{p(n,d)}{n}\, dn \approx \frac{\sigma_{noise}}{f'(t_s)} \frac{0.4\lambda}{d} \frac{1}{1 + 1.155 \log d/\lambda} \tag{44}
$$

$$
= \sigma_{noise} \frac{0.4\lambda}{d} \frac{1}{1 + 1.155 \log d/\lambda}\; t_p \;\times (0.59, 0.57, 0.54, 0.51) \qquad \text{for} \qquad n = 2, 3, 4, 5 \tag{45}
$$

$$
= \sigma_{noise} \frac{0.4\lambda}{d} \frac{1}{1 + 1.155 \log d/\lambda} \frac{1}{f_{bw}} \times (0.10, 0.12, 0.13, 0.14) \qquad \text{for} \qquad n = 2, 3, 4, 5 \tag{46}
$$

For an average cluster distance of $\lambda = 0.25\,\mu$m an amplifier with $n = 2$, this expression becomes

$$
\sigma_t = \sigma_{noise}[\text{electrons}] \times 1.6 \times 10^{-4}\, t_p \qquad d = 50\mu m \tag{47}
$$

$$
= \sigma_{noise}[\text{electrons}] \times 3.3 \times 10^{-5}\, t_p \qquad d = 200\mu m \tag{48}
$$

Assuming a 50 μm sensor and a peaking time of 2 ns and an Equivalent Noise Charge (ENC) of 50 electrons, the noise contribution to the time resolution is 16.6 ps. Assuming a 200 μm sensor and $t_p = 10$ ns and and ENC of 200 electrons, the contribution to the time resolution is 66 ps. The series noise of an amplifier for a given white series noise spectral density e_n^2 and detector capacitance C is given by

$$
\sigma_{noise}^2 = \frac{1}{2} e_n^2 C^2 \int_{-\infty}^{\infty} f'(t)^2 dt = \frac{1}{2} e_n^2\, C^2 \frac{n^2\,(2n-2)!}{t_p} \left(\frac{e}{2n}\right)^{2n} \tag{49}
$$

For constant e_n^2 the noise decreases with $1/\sqrt{t_p}$ while the time resolution is proportional to t_p, so one favours short peaking times for minimizing the impact of noise, as long as other noise sources do not become dominant.

Since we know the shape of the delta response, continuous sampling of the signal and fitting of the known shape to the sample points provides an effective way to determine the time as shown in Fig. 5a) and investigated in the following. We have to fit the function $A\, f(t - \tau)$ to the measured signal with the amplitude A and time τ as free parameters. Linearizing this expression for small values of τ we have

$$
A\, f(t - \tau) \approx A\, f(t) - A\, f'(t)\tau = \alpha_1\, f(t) - \alpha_2\, f'(t) \qquad \alpha_1 = A \qquad \alpha_2 = A\tau \tag{50}
$$

Finding the best estimate of α_1, α_2 for a signal signal $S_1, S_2, ..., S_N$ sampled at times $t_1, t_2, ..., t_N$ leads to the familiar problem of linear regression. We proceed as outlined in [24] where the problem is stated as a χ^2 minimization according to

$$
\chi^2 = \sum_{i=1}^{N} \sum_{j=1}^{N} [S_i - \alpha_1 f(t_i) + \alpha_2 f'(t_i)]\, V_{ij} [S_j - \alpha_1 f(t_j) + \alpha_2 f'(t_j)] \tag{51}
$$

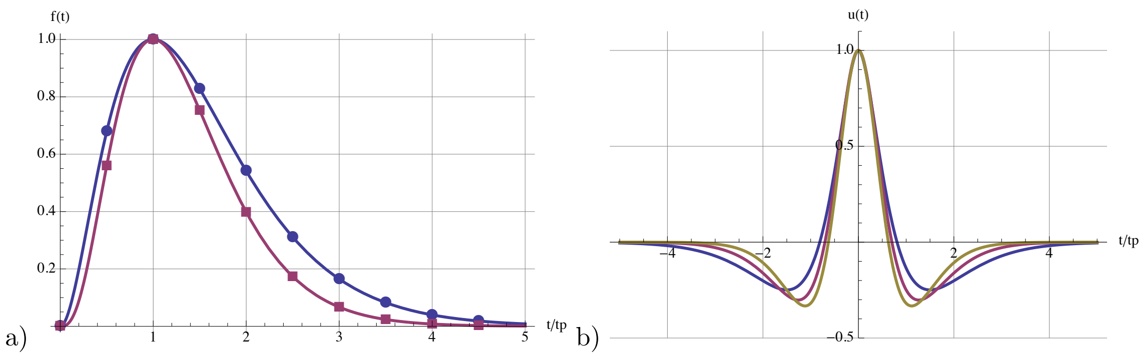

Figure 5: a) Sampling the signal at constant frequency. b) Autocorrelation function of $f'(t)$ for $n = 2, 3, 4$. For times smaller than $0.5\, t_p$ the samples become highly correlated.

The matrix V_{ij} is the inverse of the autocorrelation matrix $R_{ij} = R(t_i - t_j)$ with $R(t)$ being the autocorrelation function of the noise. The autocorrelation function of this series noise is

$$R(t) = \sigma_{noise}^2 \int_{-\infty}^{\infty} f'(t+u)\, f'(u) du = \sigma_{noise}^2\, n! \left(\frac{2n|t|}{t_p} \right)^n \frac{2t_p K_{n-1/2}(n|t|/t_p) - t K_{n+1/2}(n|t|/t_p)}{(2n-2)! \sqrt{2n|t|\, t_p \pi}} \tag{52}$$

with $K_\nu(x)$ being the modified Bessel function of the second kind. For $n = 2, 3$ evaluates to

$$R(t) = \sigma_{noise}^2 U(t) \quad = \quad \sigma_{noise}^2\, e^{-2|t|/t_p} \left[1 + 2\, \frac{|t|}{t_p} - 4 \left(\frac{|t|}{t_p} \right)^2 \right] \qquad n = 2 \tag{53}$$

$$= \quad \sigma_{noise}^2\, e^{-3|t|/t_p} \left[1 + 3\, \frac{|t|}{t_p} - 9 \left(\frac{|t|}{t_p} \right)^3 \right] \qquad n = 3 \tag{54}$$

The autocorrelation function is shown in Fig. 5b), and we see that for time intervals smaller than $t_p/2$ the samples become highly correlated. In the following we us n_s samples within the peaking time t_p, so we have sampling time bins of $\Delta t = t_p/n_s$. We sample the signal in the range of $0 < t < 5\, t_p$, giving $t_i = i\, \Delta t$ with $0 < i < 5\, n_s$. Defining

$$Q_1(n_s) = \sum_{ij} f(t_i) U_{ij}^{-1} f(t_j) \quad Q_2(n_s) = \sum_{ij} f'(t_i) U_{ij}^{-1} f'(t_j) \quad Q_3(n_s) = \sum_{ij} f'(t_i) U_{ij}^{-1} f(t_j) \tag{55}$$

where U_{ij}^{-1} is the inverse of the matrix $U_{ij} = U(t_i - t_j)$, the covariance matrix elements ε_{ij} for α_1, α_2 are then

$$\varepsilon_{11} = \sigma_A^2 = \frac{\sigma_{noise}^2\, Q_2}{Q_1 Q_2 - Q_3^2} \qquad \varepsilon_{22} = A^2\, \frac{\sigma_\tau^2}{t_p^2} = \frac{\sigma_{noise}^2\, Q_1}{Q_1 Q_2 - Q_3^2} \qquad \varepsilon_{12} = \frac{\sigma_{noise}^2\, Q_3}{Q_1 Q_2 - Q_3^2} \tag{56}$$

So for the time resolution we finally have

$$\frac{\sigma_\tau}{t_p} = \frac{\sigma_{noise}}{A} \sqrt{\frac{Q_1(n_s)}{Q_1(n_s) Q_2(n_s) - Q_3(n_s)^2}} = \frac{\sigma_{noise}}{A}\, c(n_s) \tag{57}$$

Using as before the average signal to noise ratio for a sensor of thickness d we find

$$\overline{\sigma_t} = \sigma_{noise}[\text{electrons}] \frac{0.4\lambda}{d} \, \frac{1}{1 + 1.155 \log d/\lambda}\, t_p\, c(n_s) \tag{58}$$

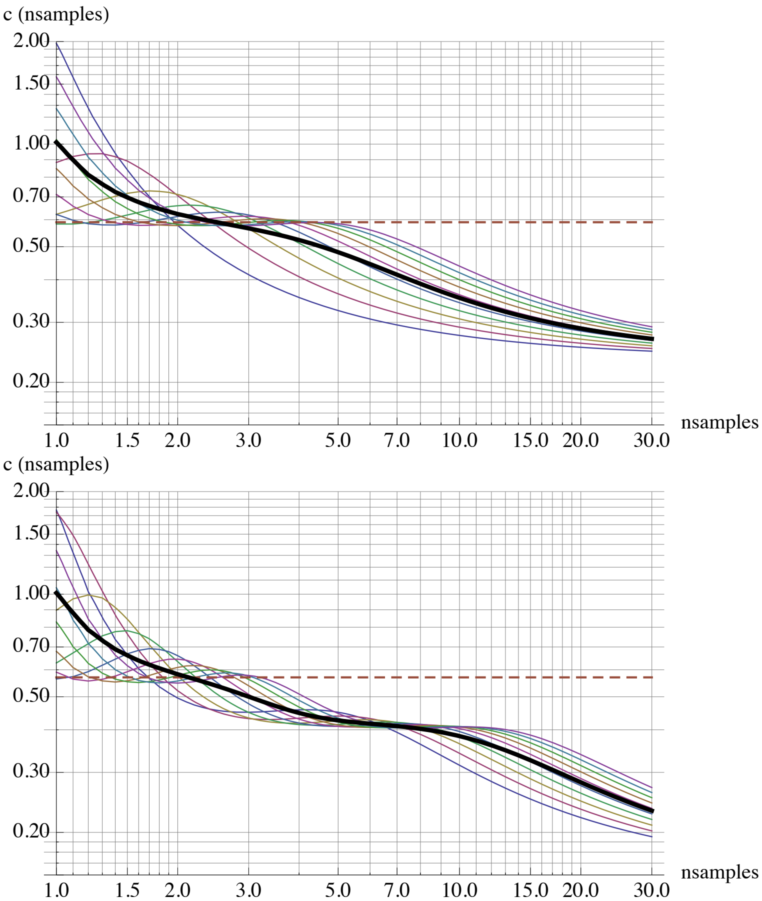

Figure 6: The function $c(n_s)$ for an amplifier with $n = 2$ (top) and $n = 3$ (bottom). The horizontal line is the result for constant fraction discrimination at the maximum slope from Eq. 45.

This expression represents the optimum time resolution that can be achieved for a given sampling frequency. Fig. 6 shows the function $c(n_s)$ assuming an amplifier with $n = 2, 3$. The horizontal lines correspond to the numbers of 0.59 and 0.57 from Eq. 45 when using constant fraction discrimination at the maximum slope. The families of curves represent a scan of the sampling phase with respect to the peak of the signal and the solid curve represents the average. The samples on the largest slope carry the highest weight on time information, while samples around the signal peak carry very little time information.

We see that sampling at an interval corresponding to half the peaking time ($n_s = 2$) gives approximately the same result as the constant fraction discrimination at maximum slope. By increasing the sampling rate further the value cannot be improved much beyond a factor 2-3. This result is quite evident, since the noise is highly correlated on a timescale of $< t_p/2$ as seen from Fig. 5b, so further increase of the sampling rate does not provide more information.

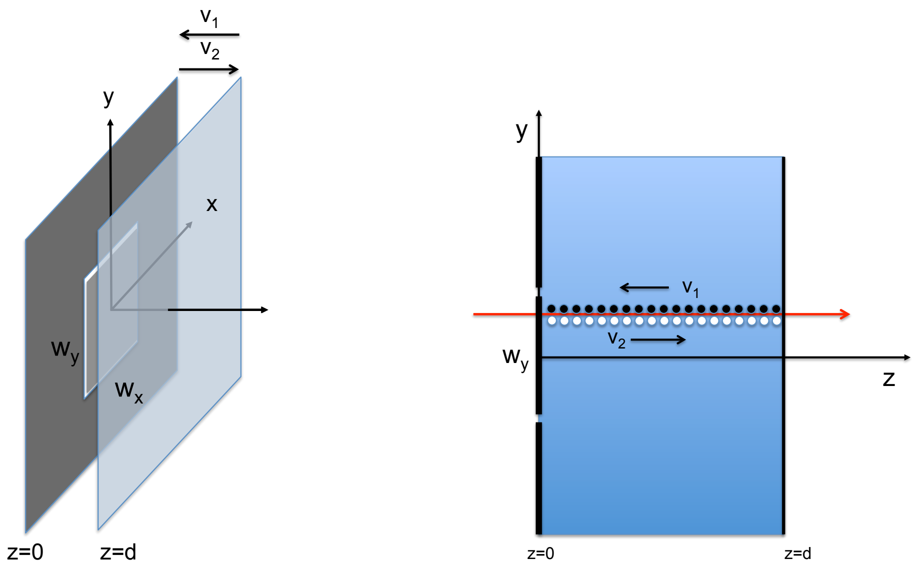

a) b)

Figure 7: a) A pixel of dimension w_x, w_y centred at $x = y = z = 0$ in a parallel plate geometry of plate distance d. b) Uniform charge deposit of a particle passing the silicon sensor. v_1 is the velocity of charges moving towards the pixel and v_2 is the velocity of charges moving away from the pixel.

6. Weighting field effect on the c.o.g. time for uniform charge deposit

Up to now we have assumed the sensor readout electrode to be represented by an infinite parallel plate capacitor, which in practice corresponds to readout pads or pixels that are much larger than then sensor thickness d. In many practical applications, the granularity is however similar to the sensor thickness. The shape of the induced signal therefore becomes dependent on the x, y position of the track and the c.o.g. time will be affected. In this section we investigate this effect by using the weighting field of a rectangular pixel as presented in [25], shown in Fig. 7a and detailed in the Appendix.
We assume again the sensor to be represented by a parallel plate geometry between $z = 0$ and $z = d$ and assume charges to move along the z-axis. We assume normal incidence of the particle and negligible diffusion. The plate at $z = 0$ is segmented into pixels such that we find a weighting field of $E_w(x, y, z) = -d\phi_w(x, y, z)/dz$ along the z-axis. We first assume a single charge pair to be produced at position z with $-q$ moving towards the the pixel at $z = 0$ according to $z_1(t) = z - v_1 t$ and $+q$ moving towards the plate at $z = d$ according $z_2(t) = z + v_2 t$, so the induced current becomes

$$\frac{i(t)}{q} = E_w[x, y, z_1(t)]\dot{z}_1(t)\,\Theta(z/v_1 - t) + E_w[x, y, z_2(t)]\dot{z}_2(t)\,\Theta((d - z)/v_2 - t) \tag{59}$$

$$= -v_1 E_w[x, y, z - v_1 t]\Theta(z/v_1 - t) - v_2 E_w[x, y, z + v_2 t]\Theta((d - z)/v_2 - t) \tag{60}$$

The c.o.g. time of this signal is

$$\tau(x, y, z) = \frac{\int t\, i(t)dt}{\int i(t)dt} = \frac{d}{v_1}\,\Psi_1(x, y, z) + \frac{d}{v_2}\,\Psi_2(x, y, z) \tag{61}$$

$$\Psi_1(x, y, z) = \frac{z}{d} - \frac{1}{d}\int_0^z \phi_w(x, y, z')dz' \qquad \Psi_2(x, y, z) = \frac{1}{d}\int_z^d \phi_w(x, y, z')dz' \tag{62}$$

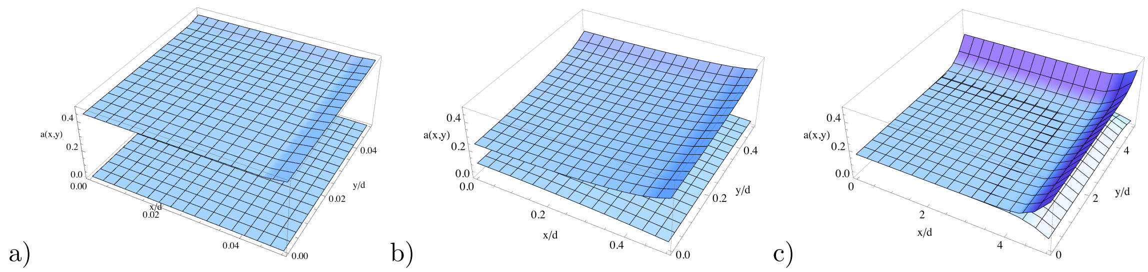

Figure 8: The functions $a_1(x,y)$ and $a_2(x,y)$ from Eq. 64 that determine the c.o.g. time for a signal from two line charges $-q_{line}, q_{line}$ at position $x, y,$. The top graph corresponds to a_1 and the bottom one to a_2. The three plots correspond to pads of size $w/d = 0.1$, $w/d = 1$, $w/d = 10$.

In case there is not a single pair of charges $q, -q$ but a pair of uniform line charges between $z = 0$ and $z = d$, as shown in Fig. 7b), we have

$$\begin{aligned} \frac{I(x,y,t)}{q_{line}} &= -v_1 \int_0^d E_w[x,y,z-v_1 t]\Theta(z/v_1 - t)dz - v_2 \int_0^d E_w[x,y,z+v_2 t]\Theta((d-z)/v_2 - t)dz \\ &= -v_1 \left[1 - \phi_w(x,y,d-v_1 t)\right]\Theta(d/v_1 - t) - v_2\, \phi_w(x,y,v_2 t)\,\Theta(d/v_2 - t) \end{aligned} \tag{63}$$

where q_{line} is the charge per unit of length. The c.o.g. time of this signal then reads as

$$\tau(x,y) = \frac{d}{v_1}\, a_1(x,y) + \frac{d}{v_2}\, a_2(x,y) = T_1\, a_1(x,y) + T_2\, a_2(x,y) \tag{64}$$

$$a_1(x,y) = \frac{1}{d}\int_0^d \Psi_1(x,y,z)dz = \frac{1}{2} - \frac{1}{d^2}\int_0^d (d-z)\phi_w(x,y,z)dz \tag{65}$$

$$a_2(x,y) = \frac{1}{d}\int_0^d \Psi_2(x,y,z)dz = \frac{1}{d^2}\int_0^d z\phi_w(x,y,z)dz \tag{66}$$

The two functions $a_1(x,y)$ and $a_2(x,y)$ are shown in Fig. 8. We can see that for large pads the values for both functions approach the constant value of 1/6 in accordance with Eq. 20 with some deviations at the border. For small pads the average of a_1 and a_2 is quite different, but the functions are also quite uniform. For the pad size of $w/d \approx 1$ the two functions vary significantly across the pad, which we will quantify next. In case the pixel is uniformly irradiated, the probability to hit an area $dx\,dy$ is given by $dx\,dy/(w_x w_y)$ and the average c.o.g. time, the second moment and the standard deviation Δ_τ are given by

$$\overline{\tau} = \frac{1}{w_x\, w_y}\int_{-w_x/2}^{w_x/2}\int_{-w_y/2}^{w_y/2} \tau(x,y)dxdy \qquad \overline{\tau^2} = \frac{1}{w_x\, w_y}\int_{-w_x/2}^{w_x/2}\int_{-w_y/2}^{w_y/2} \tau^2(x,y)dxdy \tag{67}$$

$$\Delta_\tau^2 = \overline{\tau^2} - \overline{\tau}^2 = d^2\left(\frac{c_{11}}{v_1^2} + \frac{c_{12}}{v_1 v_2} + \frac{c_{22}}{v_2^2}\right) = c_{11}T_1^2 + c_{12}T_{12} + c_{22}T_2^2 \tag{68}$$

where we have defined

$$c_{11} = \frac{1}{w_x\, w_y}\iint a_1^2 dxdy - \left(\frac{1}{w_x\, w_y}\iint a_1 dxdy\right)^2 \tag{69}$$

$$c_{12} = \frac{2}{w_x\, w_y}\iint a_1 a_2 dxdy - \frac{2}{(w_x\, w_y)^2}\iint a_1 dxdy \iint a_2 dxdy \tag{70}$$

$$c_{22} = \frac{1}{w_x\, w_y}\iint a_2^2 dxdy - \left(\frac{1}{w_x\, w_y}\iint a_2 dxdy\right)^2 \tag{71}$$

and

$$T_1 = d/v_1 \qquad T_2 = d/v_2 \qquad T_{12} = d/\sqrt{v_1 v_2} \tag{72}$$

Before moving to the numerical evaluation we investigate the limiting cases for very large and very small pads. For large pixels we have $\phi_w = 1 - z/d$ and the expressions become

$$a_1(x,y) = \frac{1}{6} \qquad a_2(x,y) = \frac{1}{6} \qquad \text{for} \qquad w/d \gg 1 \tag{73}$$

which results in $\overline{\tau} = d/6(1/v_1 + 1/v_2)$ in accordance with Eq. 20 for an infinite plane. Since there is no dependence on $x, y,$, the coefficients c_{11}, c_{12}, c_{22} vanish, which is the expected result for an infinitely large pad.

For very small pads the weighting potential falls to zero very quickly as a function of z, from it's value of unity on the pad surface at $z = 0$. The integrals of the weighting potential over z will therefore vanish and we have

$$a_1(x,y) = \frac{1}{2} \qquad a_2(x,y) = 0 \qquad \text{for} \qquad w/d \ll 1 \tag{74}$$

For this case only the charges moving towards the pad with v_1 contribute to the c.o.g. time and the average c.o.g. time becomes $\overline{\tau} = d/2v_1$. Since the weighting potential and weighting field are concentrated around the pixel surface the charges that never enter this area, i.e. the charges moving with v_2 towards $z = d$ will not contribute to the signal. The coefficients c_{11}, c_{12}, c_{22} will again vanish because a_1 and a_2 have no dependence on x, y. Because the two limiting cases are zero, this means that there will be a pad size where the effect of the weighting field fluctuation is maximal, which we see in the following.

The numerical evaluation of Eqs. 69, 70, 71 for square pixels of width w for different rations of w/d are given in Table 1 of the Appendix and the graphical representation of the coefficients is shown in in Fig. 9. The weighting potential of a pixel as given in Eq. 114 of the Appendix is used. The weighting field effect on the time resolution is worst for pad sizes corresponding to about 2-3 times the sensor thickness d, where the c_{11} and c_{12} coefficients assume a value around 2×10^{-3}. The coefficient c_{11} is related to v_1 i.e. to the charges moving to the readout pad, c_{22} is related to the charges moving in opposite direction. Since $c_{11} > c_{22}$ by a significant factor, the time resolution will be better if $v_1 > v_2$ i.e. if the electrons are moving towards the pixels. The contribution to the time resolution from Eq. 68 is shown in the Fig. 10. In case the holes move towards the pixel we find a maximum for values of $w/d \approx 2$, where the contribution becomes similar to the value from Landau fluctuations. In case the electrons move towards the pixel, the contribution is significantly smaller with maxima around $w/d \approx 1$.
The final resolution is however not given by the square sum of the Landau fluctuations from Eq. 36 and the weighting field fluctuations from Eq. 68, since there is a very strong correlation between the two. This will be discussed in the next section.

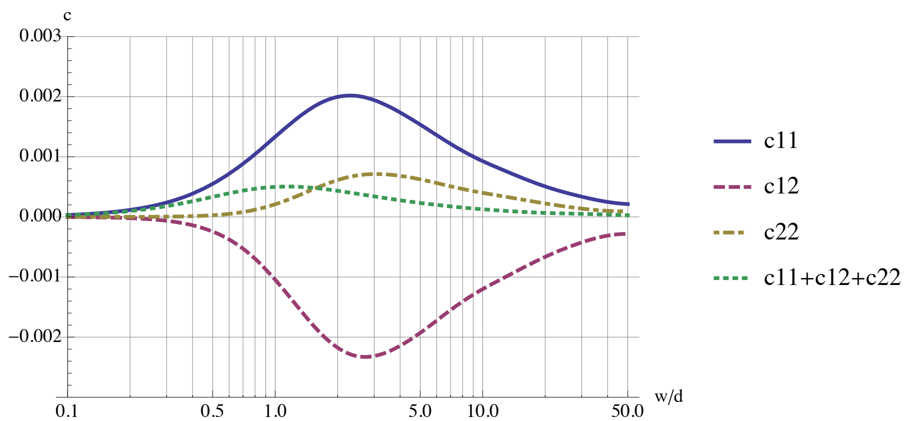

Figure 9: The coefficients c_{11}, c_{12}, c_{22} for different values of w/d, where w is the width of the square pad and d is the silicon sensor thickness.

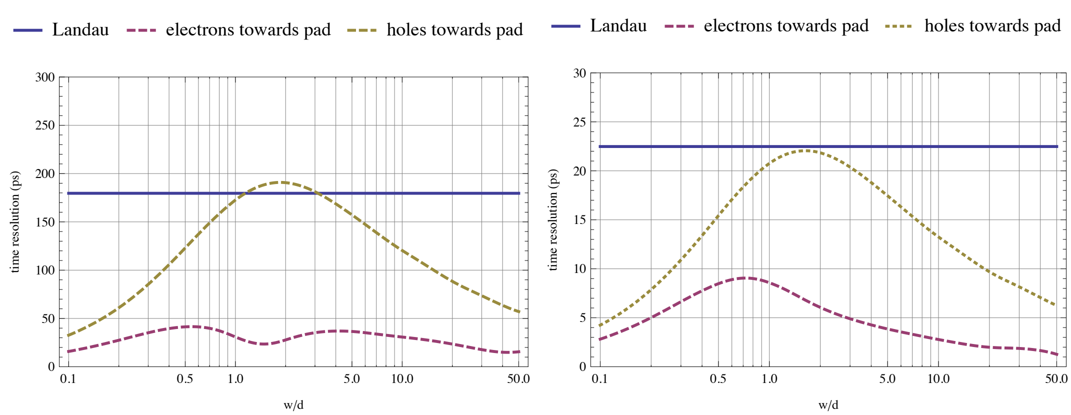

Figure 10: Standard deviation for the c.o.g. time for sensor thickness of a) $d = 200\,\mu$m and b) $d = 50\,\mu$m and $V = 200\,$V, assuming uniform charge deposit and a square readout pad. The horizontal line represents c.o.g. time resolution from Eq. 36 due to Landau fluctuations only. The two curves in the plots represent the effect of weighting field fluctuations where either the electrons or the holes move towards the readout pad.

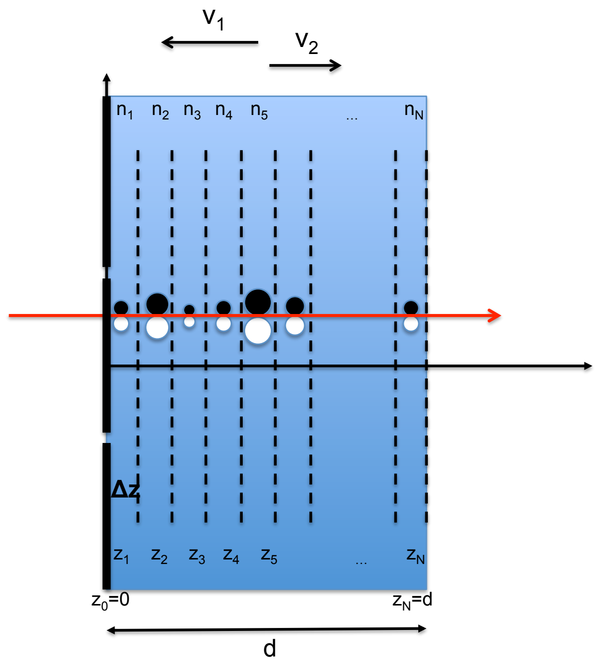

Figure 11: Silicon sensor with a readout pad centered at $x = y = z = 0$. v_1 is the velocity of charges moving towards the pixel and v_2 is the velocity of charges moving away from the pixel.

7. C.o.g. time resolution for combined charge fluctuations and weighting field fluctuations

In this section we consider the Landau fluctuations together with the variation of the x, y position of the particle trajectory and the related fluctuation of the weighting field. The center of gravity time for a particle that passes the sensor at position x, y and deposits n_k charges in the N detector slices is given by

$$\tau(n_1, n_2, ..., n_N, x, y) = \frac{1}{\sum_{k=1}^N n_k} \sum_{k=1}^{N} n_k \tau(x, y, k\Delta z) \tag{75}$$

where $\tau(x, y, z)$ is from Eq. 61. Proceeding as before we have to calculate $\overline{\tau}$ and $\overline{\tau^2}$, where in addition to the integrals over $dn_1, dn_2, ..., dn_N$ we have to perform the integral $1/(w_x w_y) \int\int \tau dxdy$ for uniform illumination of a pad, and the final result for the variance is

$$\begin{aligned} \overline{\tau^2} - \overline{\tau}^2 \quad &= \quad \frac{b_N\, d}{\Delta z} \frac{1}{w_x w_y} \iint \left[\frac{1}{d} \int_0^d \tau(x, y, z)^2 dz - \left(\frac{1}{d} \int_0^d \tau(x, y, z) dz \right)^2 \right] dxdy \qquad (76) \\ &+ \quad \frac{1}{w_x w_y} \iint \left(\frac{1}{d} \int_0^d \tau(x, y, z) dz \right)^2 dxdy - \left[\frac{1}{w_x w_y} \iint \left(\frac{1}{d} \int_0^d \tau(x, y, z) dz \right) dxdy \right]^2 \end{aligned}$$

The second line of the expression is equivalent to the one considering the weighting field effect without charge fluctuations from the previous section, so the result can be expressed in the following terms

$$\Delta_\tau^2 = \frac{b_N\, d}{\Delta z} d^2 \left(\frac{k_{11}}{v_1^2} + \frac{k_{12}}{v_1 v_2} + \frac{k_{22}}{v_2^2} \right) + d^2 \left(\frac{c_{11}}{v_1^2} + \frac{c_{12}}{v_1 v_2} + \frac{c_{22}}{v_2^2} \right) \tag{77}$$

with $b_N\,d/\Delta z = 1/(1+1.155\log d/\lambda)$ for the Landau fluctuations. The coefficients c_{11}, c_{12}, c_{22} are the ones from the previous chapter and the coefficients k_{11}, k_{12}, k_{22} are given by

$$k_{11} = \frac{1}{w_x w_y}\iint (b_{11}-a_1^2)dxdy \qquad k_{12} = \frac{2}{w_x w_y}\iint (b_{12}-a_1 a_2)dxdy \qquad k_{22} = \frac{1}{w_x w_y}\iint (b_{22}-a_2^2)dxdy \tag{78}$$

with

$$b_{11}(x,y) = \frac{1}{d}\int_0^d \Psi_1(x,y,z)^2 dz = \frac{1}{d}\int_0^d \left[\frac{z}{d} - \frac{1}{d}\int_0^z \phi_w(x,y,z')dz'\right]^2 dz \tag{79}$$

$$b_{12}(x,y) = \frac{1}{d}\int_0^d \Psi_1(x,y,z)\Psi_2(x,y,z)dz = \frac{1}{d}\int_0^d \left[\frac{z}{d} - \frac{1}{d}\int_0^z \phi_w(x,y,z')dz'\right]\left[\frac{1}{d}\int_z^d \phi_w(x,y,z')dz'\right] dz$$

$$b_{22}(x,y) = \frac{1}{d}\int_0^d \Psi_2(x,y,z)^2 dz = \frac{1}{d}\int_0^d \left[\frac{1}{d}\int_z^d \phi_w(x,y,z')dz'\right]^2 dz$$

First we verify that the limiting cases for very large pads and very small pads. For large pads we substitute for the weighting potential the expression $\phi_w(x,y,z) = 1 - z/d$ and find

$$b_{11}(x,y) = \frac{1}{20} \qquad b_{12}(x,y) = \frac{1}{120} \qquad b_{22}(x,y) = \frac{1}{20} \qquad w/d \gg 1 \tag{80}$$

which gives $k_{11} = k_{22} = 4/180, k_{12} = -7/180$ and $c_{11} = c_{12} = c_{22} = 0$, so we recuperate Eq. 31. For very small pads the integrals of the weighting potential over z will again vanish as discussed before, and we have

$$b_{11}(x,y) = \frac{1}{3} \qquad b_{12}(x,y) = 0 \qquad b_{22}(x,y) = 0 \qquad w/d \ll 1 \tag{81}$$

which gives $k_{11} = 1/12, k_{12} = k_{22} = 0$ and $c_{11} = c_{12} = c_{22} = 0$ and therefore have

$$\Delta_\tau = \sqrt{\frac{b_N\,d}{\Delta z}}\,\frac{T_1}{\sqrt{12}} \tag{82}$$

For small pads the weighting potential decays very quickly fas a function of z, from its value of 1 on the pad surface to zero. The weighting field, which defines the induced current, is therefore very large close to the pad and zero for larger values of z. Only when the charges arrive at this position they will induce a signal. In the limiting case this is equivalent to a delta current signal for each charge that arrives at $z = 0$, and we have

$$i(t) = q\sum_{k=1}^{N} n_k\,\delta(t - k\Delta z/v_1) \qquad \tau = \frac{1}{\sum_{k=1}^{N} n_k}\sum_{k=1}^{N} n_k\,k\Delta z/v_1 \qquad \Delta_\tau = \sqrt{\frac{b_N\,d}{\Delta z}}\,\frac{T_1}{\sqrt{12}} \tag{83}$$

so we indeed recuperate the above expression for Δ_τ ! We'll see the same formula later in Eq. 100 for silicon sensors with gain.

The coefficients k_{11}, k_{12}, k_{22} for square pads are listed in Table 2 of the Appendix and are shown in Fig. 12. The factor k_{11}, related to the charges moving with v_1 towards the pixel, is again larger than k_{22}, so as stated before the resolution is better if the electrons move towards the pixel. This fact is illustrated in Fig. 13 and Fig. 14 for a $200\,\mu$m and $50\,\mu$m sensor. It shows a significant difference for these two scenarios. In case the electrons move to the pixel the weighting field effect seems not to add significantly to the time resolution for values of $w/d \gtrsim 1$.

For pads with $w/d > 20$ one approaches the scenario of an infinitely extended electrode, as expected. For smaller pixels the resolution is significantly worse than expected from the quadratic sum of the weighting field effect for uniform charge deposit and the Landau fluctuation effects assuming an infinitely large electrode.

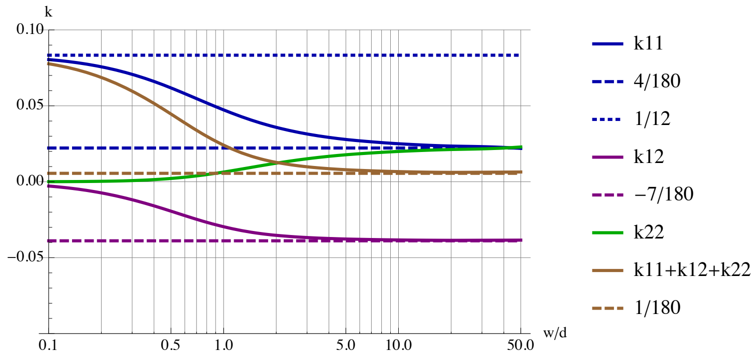

Figure 12: The coefficients k_{11}, k_{12}, k_{22} for different values of w/d, where w is the width of the square pad and d is the silicon thickness. The dotted lines represent the for very small pads and very large pads as discussed in the text.

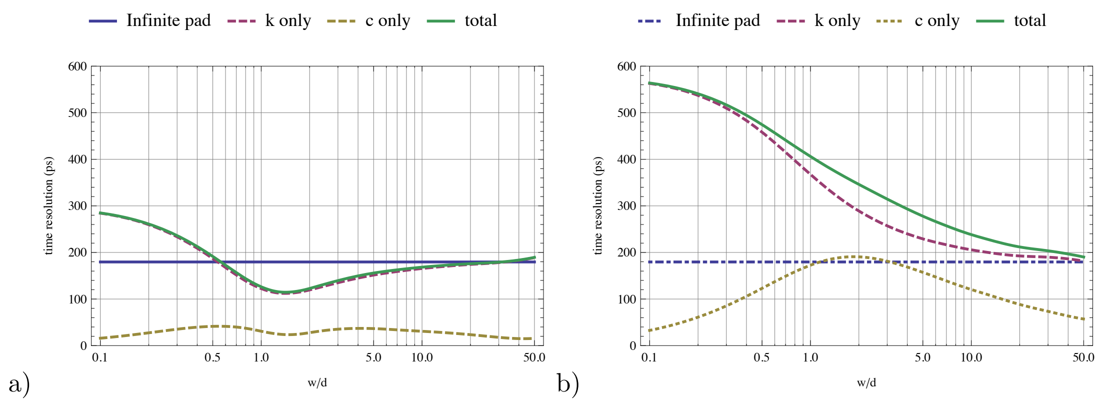

Figure 13: C.o.g. time resolution for values of $d = 200\,\mu$m and $V = 200\,$V as a function of the pixel size w. The 'c only' curve refers to the effect from a uniform line charge. In a) the electrons move towards the pixel while in b) the holes move towards the pixel.

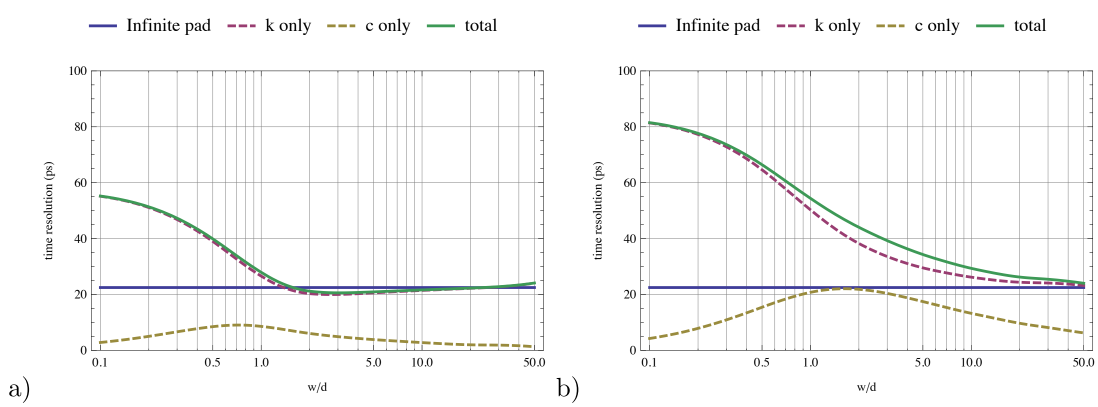

Figure 14: Time resolution for values of $d = 50\,\mu$m and $V = 200\,$V as a function of the pixel size w. The 'c only' curve refers to the effect from a uniform line charge. In a) the electrons move towards the pixel while in b) the holes move towards the pixel.

8. Leading edge discrimination

Up to this point we have just discussed the center of gravity time of the detector signals. In this section we consider the measured time to be determined by leading edge discrimination of the normalized detector signal. We process the detector signal by an amplifier of a given peaking time, and perform the so called 'slewing correction' for eliminating the timewalk effect from pulseheight fluctuations by dividing the amplifier output signal by the total signal charge and set the threshold to a given fraction of this signal. The current signal due to a single charge pair $-q, q$at position x, y, z is

$$i_0(x,y,z,t) = -q\left[v_1\, E_w(x,y,z-v_1t)\Theta(z/v_1-t) + v_2\, E_w(x,y,z+v_2t)\Theta((d-z)/v_2-t)\right] \tag{84}$$

The current signal for having n_1 e/h pairs at $z=\Delta z$, n_2 e/h pairs at $z=2\Delta z$ etc. is given by

$$i(n_1,n_2,...,n_N,x,y,t) = \sum_{k=1}^{N} n_k i_0(x,y,k\Delta z,t) \tag{85}$$

We now process this signal by an amplifier with delta response $cf(t/t_p)$ where t_p is the peaking time, $f(1)=1$, c is the amplifier sensitivity in units of $[V/C]$ and $f(x)$ is defined by

$$f(x) = x^n\, e^{n(1-x)} \tag{86}$$

The amplifier output signal becomes

$$\begin{aligned} s(n_1,n_2,...,n_N,x,y,t) &= c\int_0^t f\left(\frac{t-t'}{t_p}\right) i(n_1,n_2,...,n_N,x,y,t')dt' && (87)\\ &= c\,q\sum_{k=1}^{N} n_k\, g(x,y,k\Delta z,t) && (88) \end{aligned}$$

where $g(x,y,z,t)$ is given by

$$\begin{aligned} g(x,y,z,t) &= \Theta(z-v_1t)\int_{\frac{z-v_1t}{d}}^{\frac{z}{d}} f\left(\frac{v_1t-z+ud}{v_1t_p}\right) E_w^z(x/d,y/d,u,w_x/d,w_y/d,1)du && (89)\\ &+ \Theta(v_1t-z)\int_0^{\frac{z}{d}} f\left(\frac{v_1t-z+ud}{v_1t_p}\right) E_w^z(x/d,y/d,u,w_x/d,w_y/d,1)du\\ &+ \Theta[(d-z)-v_2t]\int_{\frac{z}{d}}^{\frac{z+v_2t}{d}} f\left(\frac{v_2t+z-ud}{v_2t_p}\right) E_w^z(x/d,y/d,u,w_x/d,w_y/d,1)du\\ &+ \Theta[v_2t-(d-z)]\int_{\frac{z}{d}}^{1} f\left(\frac{v_2t+z-ud}{v_2t_p}\right) E_w^z(x/d,y/d,u,w_x/d,w_y/d,1)du \end{aligned}$$

The weighting field $E_w^z(x,y,z,w_x,w_y,d)$ for a pixel is given in Eq. 119 of the Appendix. To perform slewing corrections we divide the signal by the total charge $q\sum n_k$ and we get the normalized amplifier output signal

$$h(n_1,n_2,...,n_N,x,y,t) = \frac{c}{\sum_{k=1}^{N} n_k}\sum_{k=1}^{N} n_k\, g(x,y,k\Delta z,t) \tag{90}$$

The averaged normalized signal and the variance of the signal evaluate to

$$\overline{h}(t) = \frac{c}{w_x\,w_y}\iint\left[\int_0^1 g(x,y,sd,t)ds\right]dxdy \tag{91}$$

and

$$\Delta_h^2(t) = \frac{b_N\, d}{\Delta z}\frac{c^2}{w_x w_y}\iint \left[\int_0^1 g(x,y,sd,t)^2 ds - \left(\int_0^1 g(x,y,sd,t)ds\right)^2\right] dxdy$$
$$+ \frac{c^2}{w_x w_y}\iint \left(\int_0^1 g(x,y,sd,t)ds\right)^2 dxdy - \left[\frac{c}{w_x w_y}\iint \left(\int_0^1 g(x,y,sd,t)ds\right) dxdy\right]^2 \quad (92)$$

The time resolution is then defined by (Fig. 15b)

$$\sigma_t = \frac{\Delta_h(t)}{\overline{h}'(t)} \quad (93)$$

Here we just discuss the example of an infinitely extended pixel i.e. we use $E_w^z(x,y,z,w_x,w_y,d) = 1/d$, which evaluates $g(x,y,z,t)$ to

$$\begin{aligned}
\frac{n^{n+1}}{e^n}\frac{d}{t_p}\, g(x,y,z,t) &= v_1\,\Theta(z - v_1 t)\,[n! - \Gamma(n+1, t/t_p)] \\
&- v_1\,\Theta(v_1 t - z)\,[\Gamma(n+1,t/t_p) - \Gamma(n+1, -(z - v_1 t)/(t_p v_1)] \\
&+ v_2\,\Theta((d-z) - v_2 t)\,[n! - \Gamma(n+1, t/t_p] \\
&- v_2\,\Theta(v_2 t - (d-z))\,[\Gamma(n+1,t/t_p) - \Gamma(n+1, -(d - z - v_2 t)/(t_p v_2)]
\end{aligned}$$

where n and t_p are the parameters defining the amplifier. As an example the average signal $\overline{h}(t)$ for a $50\,\mu$m sensor at 200 V for different peaking times is shown in Fig. 15a). The signal duration is around 0.8 ns, so for small peaking times of 0.25 and 0.5 ns there is significant 'ballistic deficit' while for peaking times > 1 ns the amplifier 'integrates' the full signal and the normalized amplitude becomes unity. In Fig. 15b) the average normalized signal for a peaking time of 0.25 ns is shown, together with ± 1 standard deviations.
The resulting time resolution is the shown in Fig. 16a) and Fig. 17a) for a $50\,\mu$m and a $200\,\mu$m sensor. We find that for large peaking times, the time resolution indeed approaches the c.o.g. time value, while for smaller peaking times the time resolution can be significantly better when setting the threshold at less than 30-40% of the normalized signal. E.g. for the $50\,\mu$m sensor at 200 V, a peaking time of 0.25 ns and a threshold set to 40% of the total signal charge one should even arrive at 12 ps time resolution. For a $200\,\mu$m sensor one expects a time resolution of < 100 ps for $t_p = 5$ ns and a threshold at 30% of the signal.

To study the impact of the noise we assume σ_{noise} to be given in units of electrons. This noise is superimposed to the signal $s(t)$ from E.q 87, so when normalizing the signal to arrive at $h(t)$ we also have to normalize the noise by the total amount of charge deposited in the sensor. The average normalized noise the becomes

$$\overline{\sigma}_{norm} = \int_0^\infty \frac{\sigma_{noise}}{n} p(n,d)\, dn = \sigma_{noise}\,\frac{\lambda}{2.50\, d}\,\frac{1}{1 + 1.155\log d/\lambda} \quad (94)$$

The contribution of the noise to the time resolution is then

$$\sigma_t = \frac{\overline{\sigma}_{norm}}{\overline{h}'(t)} \quad (95)$$

We can therefore express the required noise level when using a threshold of $\overline{h}(t)$, that matches the resolution from Landau fluctuations from Eq. 93, as

$$\sigma_{noise}[electrons] = \Delta_h(t)\,\frac{2.50\, d}{\lambda}\,(1 + 1.155\log d/\lambda) \quad (96)$$

The numbers are shown in Fig. 16b) and Fig. 17b). For the $50\,\mu$m sensor and $t_p = 0.25$ ns the required noise level is 100 electrons and for the $200\,\mu$m sensor at $t_p = 5$ ns the required noise is 400 electrons.

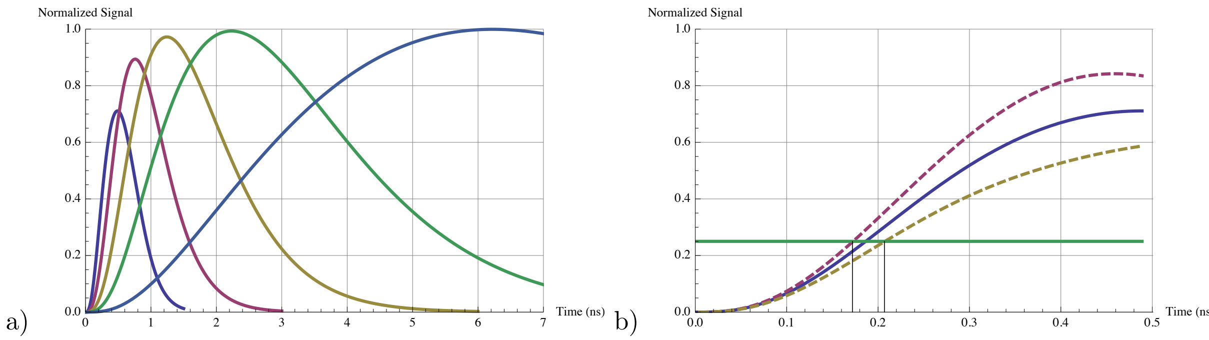

Figure 15: a) Average normalized signal $\overline{h}(t)$ for amplifier peaking times $t_p = 0.25, 0.5, 1, 2, 6\,$ns for a 50μm sensor and V=200 V. b) The normalized average signal $\overline{h}(t)$ for $t_p = 0.25\,$ns together with the curves $\overline{h}(t) + \Delta_h(t)$ and $\overline{h}(t) - \Delta_h(t)$.

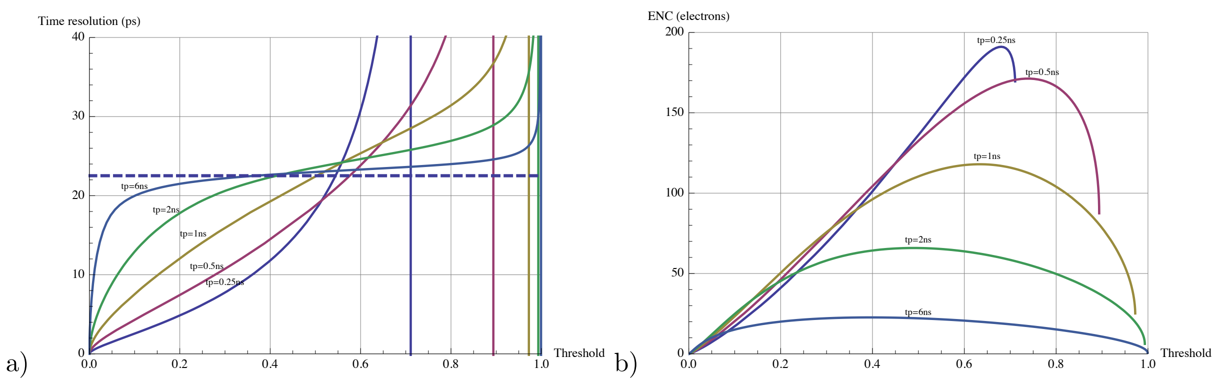

Figure 16: a) Time resolution for a sensor of 50μm thickness at 200 V bias voltage. The slewing correction is performed by dividing the signal by the total charge and applying the threshold as a fraction of this charge. b) ENC needed to match the noise effect on the time resolution to the effect from the Landau fluctuations.

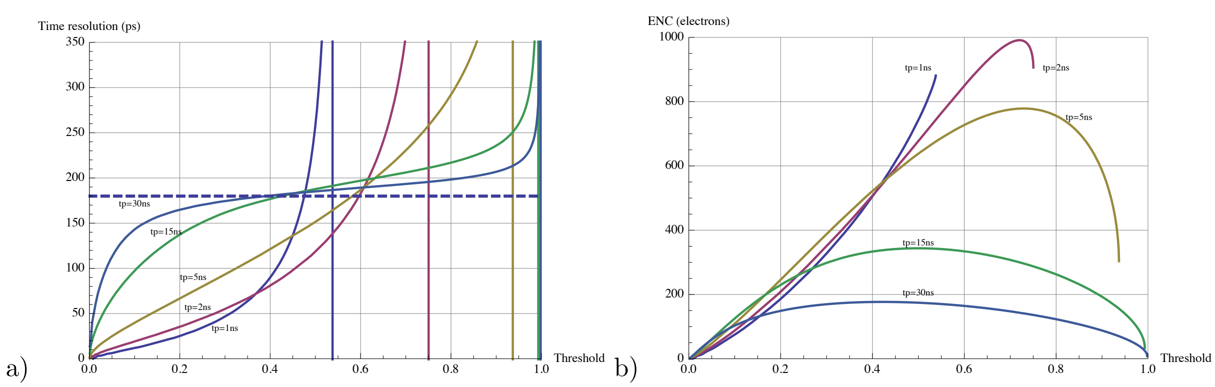

Figure 17: a) Time resolution for a sensor of 200μm thickness at 200 V bias voltage. The slewing correction is performed by dividing the signal by the total charge and applying the threshold as a fraction of this charge. b) ENC needed to match the noise effect on the time resolution to the effect from the Landau fluctuations.

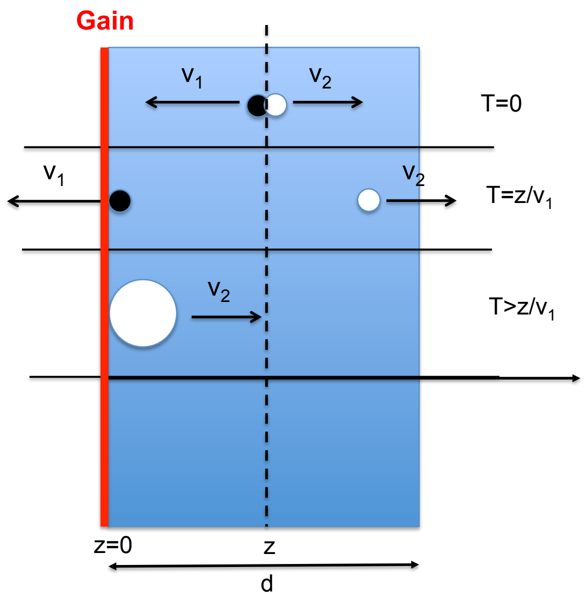

Figure 18: Silicon sensor with internal gain. An e-h par is produced at position z, the electron arrives at $z = 0$ at time $T = z/v_1$, the electron multiplies in a high field layer at $z = 0$ and the holes move back to $z = d$, inducing the dominant part of the current signal.

9. Silicon sensors with internal gain

In the Low Gain Avalanche Diode (LGAD), a high field region is implemented in the sensor in order to multiply electrons at some moderate gain and as a result improve the signal to noise ratio. We assume the geometry from Fig. 1 with the amplification structure located at $z = 0$. The electrons will therefore move from their point of creation to this structure, get multiplied and the holes created in the multiplication process are moving back from $z = 0$ to $z = d$ through the entire sensor thickness d. If we assume 1) the gain G to be sufficiently large such that the signal from the primary electron and hole movement is negligible, 2) the amplification structure to be infinitely thin, 3) a sensor with negligible depletion voltage, the signal from a single e-h pair created at position z is of rectangular shape with duration $T = d/v_2$, shifted by the time $t = z/v_1$

$$i(t) = -G\,\frac{q\,v_2}{d}\,[\Theta(t - z/v_1) - \Theta(t - z/v_1 - d/v_2)] \tag{97}$$

The c.o.g. time of this signal is

$$\tau = \frac{d}{2v_2} + \frac{z}{v_1} \tag{98}$$

The signal for the case of $n_1, n_2, ..., n_N$ clusters at positions $z_1, z_2, ..., z_N$ is then

$$\tau(n_1, n_2, ..., n_N) = \frac{1}{\sum_{k=1}^{N} n_k} \sum_{k=1}^{N} n_k \left(\frac{d}{2v_2} + \frac{z_k}{v_1}\right) = \frac{d}{2v_2} + \frac{1}{\sum_{k=1}^{N} n_k} \sum_{k=1}^{N} n_k \frac{z_k}{v_1} \tag{99}$$

The average and standard deviation of the c.o.g. time is then

$$\overline{\tau} = \frac{d}{2}\left(\frac{1}{v_1} + \frac{1}{v_2}\right) \qquad \Delta_\tau = \sqrt{\frac{b_N\,d}{\Delta z}\,\frac{d^2}{12v_1^2}} = \frac{1}{\sqrt{1 + 1.155\log d/\lambda}}\,\frac{T_1}{\sqrt{12}} \tag{100}$$

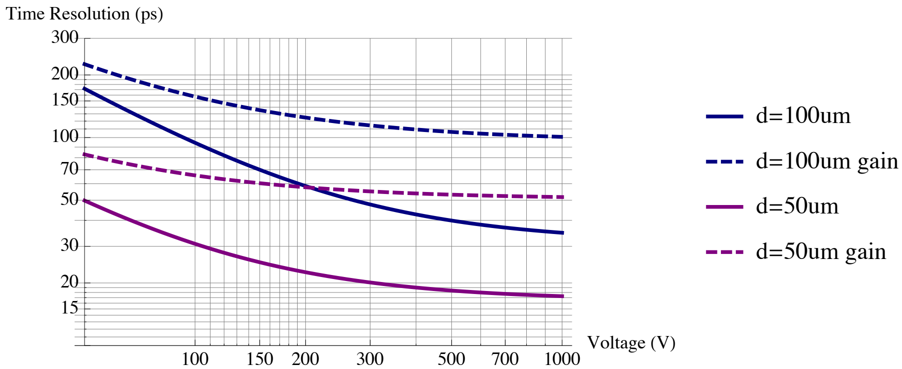

Figure 19: Standard deviation of the c.o.g. time from Eq. 36 for 50μm and 100 μm thickness for standard sensors (solid) and from Eq. 100 for and LGAD sensor with internal gain of electrons assuming a signal only from gain holes (dashed).

with $T_1 = d/v_1$ being the total electron drift time. This expression is the same as the one from Eq. 82 and Eq. 83, so this sensor is simply measuring the arrival time distribution of the electrons at $z = 0$. The variance is significantly larger than the one for the sensor without gain, as shown in Fig. 19 for a sensor thickness of 50 and 100 μm. E.g. for a 50 μm sensor the c.o.g. time resolution without gain is 23 ps while for a sensor with gain it is around 60 ps.

The effects defining the time resolution for a sensor with gain therefore differ significantly from one without gain. The electrons first have to arrive at $z = 0$ before being amplified an producing the gain signal, so the signal timing is defined by the arrival time distribution of the electron clusters at $z = 0$. This is also illustrated by the fact that the second factor in Eq. 100 is simply the total transit time $T_e = d/v_1$ of the electrons through the full silicon thickness divided by $\sqrt{12}$. For the LGAD the c.o.g. time is therefore not a good way to exploit the timing and it is essential to use fast electronics in order to catch the signal from the very first arriving electron clusters.

10. Weighting field effect on the c.o.g. time for silicon sensors with gain

For completion we discuss the effect of the finite pixel size on the c.o.g. time resolution for sensors with gain. Assuming the readout electrode at $z = 0$ to be segmented into pixels with an associated weighting potential $\phi_w(x, y, z)$, the induced signal due to a single charge pair created at position z at $t = 0$ becomes

$$i(t) = -G\, q\, v_2\, E_w[x, y, v_2(t - z/v_1)]\, [\Theta(t - z/v_1) - \Theta(t - z/v_1 - d/v_2)] \tag{101}$$

and the c.o.g. time for this signal is given by

$$\tau(x, y, z) = \frac{z}{v_1} + \frac{d}{v_2} \int_0^1 \phi_w(x, y, s\, d) ds \tag{102}$$

Assuming a uniform charge deposit along the track, the c.o.g. time becomes

$$\tau(x, y) = \frac{1}{d} \int_0^d \tau(x, y, z) dz = \frac{d}{2v_1} + \frac{d}{v_2} \int_0^1 \phi_w(x, y, s\, d) ds \tag{103}$$

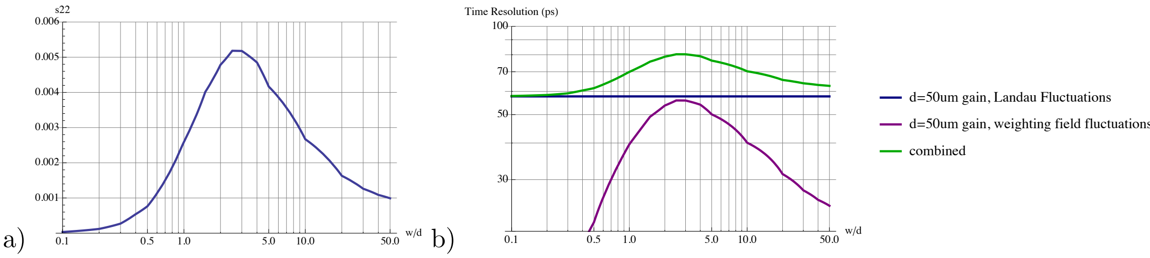

Figure 20: a) Coefficient s_{22} defining the impact on of the weighting field on the time resolution. b) C.o.g. time resolution for a gain sensor of $50\,\mu$m thickness at 200 V. The horizontal line shows the contribution from Landau fluctuations only, while the other lines show the contribution from weighting field fluctuations as well as the combined effect.

The variance for uniform irradiation of the pad is then

$$\begin{aligned}\Delta_\tau^2 &= \overline{\tau^2} - \overline{\tau}^2 \\ &= \frac{d^2}{v_2^2}\left[\frac{1}{w_x w_y}\iint\left(\int_0^1 \phi_w(x,y,s\,d)ds\right)^2 dxdy - \left(\frac{1}{w_x w_y}\iint\left(\int_0^1 \phi_w(x,y,s\,d)ds\right)dxdy\right)^2\right] \\ &= \frac{d^2}{v_2^2}\,s_{22} = T_2^2\,s_{22} \end{aligned} \tag{104}$$

which is the pendant to Eq. 68 for sensors without gain. The coefficient s_{22} for different pixel sizes is shown in Fig. 20 a). The effect on the time resolution for a $50\,\mu$m sensor is shown in Fig. 20 b). The effect is again largest for pixel sizes of $w/d \approx 3$. In case we also take into account the Landau fluctuations we have to use Eq. 102 in Eq. 76 and find

$$\Delta_\tau^2 = \overline{\tau^2} - \overline{\tau}^2 = \frac{b_N d}{\Delta z}\frac{d^2}{12\,v_1^2} + \frac{d^2}{v_2^2}s_{11} = \frac{b_N d}{\Delta z}\frac{T_1^2}{12} + T_2^2 s_{22} \tag{105}$$

which is the pendant to Eq. 77 for sensors without gain. So we find the interesting result that in this case there is no correlation between the Landau fluctuations and the weighting field fluctuations and the two components just add in squares. We also note that the result will be the same whether we segment the electrode at $z=0$ where the multiplication takes place or whether we segment the electrode at $z=d$.

11. Leading edge discrimination for silicon sensors with gain

We finally discuss the time resolution when considering leading edge discrimination of sensors with gain. We proceed as before and convolute the signal from a single e-h pair at position z

$$i_0(x,y,z,t) = -Gqv_2E_w(x,y,v_2(t-z/v_1))\left[\Theta(t-z/v_1) - \Theta(t-z/v_1-d/v_2)\right] \tag{106}$$

with the electronics delta response and find

$$\begin{aligned} g(x,y,z,t) &= \Theta(t-z/v_1)\Theta(d/v_2+z/v_1-t)\int_0^{\frac{v_2}{d}(1-\frac{z}{v_1})} f\left(\frac{t-z/v_1-ud/v_2}{t_p}\right)E\left(\frac{x}{d},\frac{y}{d},u,\frac{w_x}{d},\frac{w_y}{d},1\right)du \\ &+ \Theta(t-d/v_2-z/v_1)\int_0^1 f\left(\frac{t-z/v_1-ud/v_2}{t_p}\right)E\left(\frac{x}{d},\frac{y}{d},u,\frac{w_x}{d},\frac{w_y}{d},1\right)du \end{aligned} \tag{107}$$

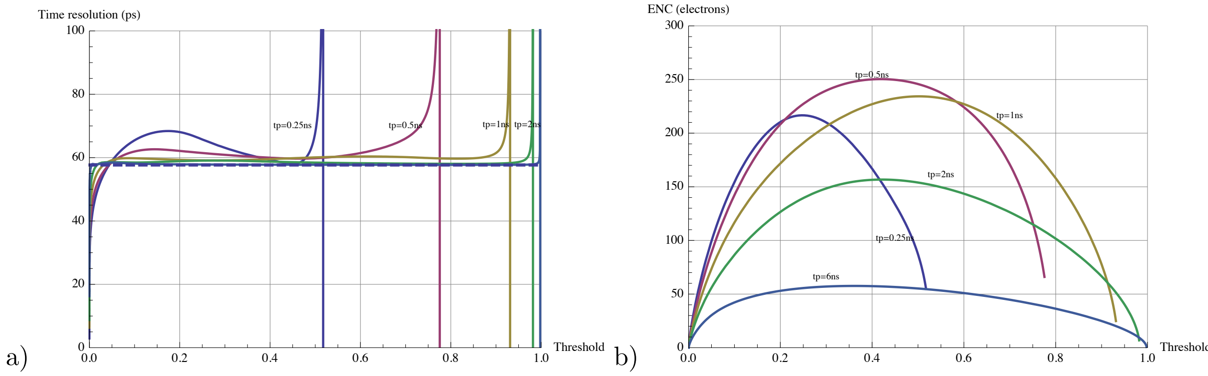

Figure 21: a) Time resolution for a gain sensor of 50μm thickness at 200 V bias voltage when applying a threshold to the signal normalized by the total charge. The values do not improve beyond the c.o.g. time resolution number. b) ENC needed to match the noise effect of the time resolution to the effect from the Landau fluctuations.

which for an infinitely extended electrode with $E_w = 1/d$ evaluates to

$$\begin{aligned}\frac{n^{n+1}}{e^n}\frac{d}{t_p}\,g(x,y,z,t) &= v_2\Theta(t-z/v_1)\Theta(d/v_2+z/v_1-t)\left[n! - \Gamma\left(n+1,\frac{n(v_1 t - z)}{t_p v_1}\right)\right] \\ &- v_2\Theta(t-d/v_2-z/v_1)\left[\Gamma\left(n+1,\frac{n(v_1 t-z)}{t_p v_1}\right) - \Gamma\left(n+1,\frac{n(t-d/v_2-z/v_1)}{tp}\right)\right]\end{aligned} \tag{108}$$

Evaluating Eq. 91, Eq. 92 and Eq. 93 we then find the results shown in Fig. 21a). We find that even for leading edge discrimination of the normalized signal the time resolution for a sensor with gain does not improve beyond the c.o.g. time resolution value. The reason is that in the outlined formulas the signal is normalized by the total charge deposited in the sensor. The signal that makes up the leading edge has however no correlation with the total deposited charge but is only related to the number of electrons that have already arrived at the gain layer. This is very different from the standard silicon sensor without gain, where the movement of all deposited charges makes up the leading edge signal.
For the sensors with gain, the slewing correction must therefore be related to the slope of the leading edge and not to the total charge of the signal. Double threshold or classical constant fraction discriminators are therefore necessary to fully exploit the time resolution of these sensors. This goes beyond the mathematical formalisms developed in this report and Monte Carlo simulations of this scenario might be more efficient.

12. Conclusions

We have derived analytic expressions for the time resolution of silicon sensors.

- The standard deviation of the center of gravity (c.o.g.) time of a silicon detector signal is given by

$$\Delta_\tau = \frac{1}{\sqrt{1 + 1.155 \log d/\lambda}} \sqrt{\frac{4}{180} T_1^2 - \frac{7}{180} T_{12}^2 + \frac{4}{180} T_2^2} \tag{109}$$

  assuming a large readout electrode, the Landau distribution for charge deposit and negligible depletion voltage. d is the sensor thickness and λ is the average distance between primary collisions, which evaluates to $\approx 0.25\,\mu$m for relativistic particles. $T_1 = d/v_1, T_2 = d/v_2, T_{12} = d/\sqrt{v_1 v_2}$ are the drift times of the electrons and holes. This evaluates to $\Delta_\tau = 370$, 180, 59, 23 ps for sensor thickness values of 300, 200, 100, 50 μm and assuming 200 V applied with negligible depletion voltage. We note that the Landau distribution tends to overestimate the charge fluctuations and that the time distribution is quite non-gaussian, so these numbers might be slightly pessimistic.

- Measuring the sensor signal with an amplifier of peaking time t_p larger than the drift time of electrons and holes, the amplifier output is equal to the delta response, scaled by the total signal charge and shifted by the c.o.g. time. To determine the time of this pulse of known shape one can then use standard techniques of constant fraction discrimination and optimum filtering to extract the time information. The average contribution of the noise to the time resolution is then

$$\overline{\sigma}_t = \sigma_{noise}[electrons] \frac{0.4\lambda}{d} \frac{1}{1 + 1.55 \log d/\lambda}\, t_p\, c(n_s) \tag{110}$$

  where t_p is the peaking time of the amplifier and $c(n_s)$ is a constant depending on the measurement technique. Using constant fraction discrimination at the maximum slope of the signal we have $c(n_s) \approx 0.55 - 0.6$. Using continuous signal sampling and optimum filtering one arrives at similar numbers when sampling at an interval of $t_p/2$ and one can achieve $c(n_s) \approx 0.2 - 0.3$ for very high frequency sampling. For $t_p = 2$ ns, $d = 50\,\mu$m and an Equivalent Noise Charge of 50 electrons we have a contribution from the noise of $\sigma_t \approx 17$ ps, that has to be added in squares with the above number of 23 ps from Landau fluctuations.

- Assuming a square readout pixel of dimension w, the variation the track position and therefore the variation of the weighting field and related signal shape will have an impact on the time resolution and the standard deviation of the c.o.g. time becomes

$$\Delta_\tau = \sqrt{\frac{k_{11} T_1^2 + k_{12} T_{12}^2 + k_{22} T_2^2}{1 + 1.155 \log d/\lambda} + (c_{11} T_1^2 + c_{12} T_{12}^2 + c_{22} T_2^2)} \tag{111}$$

  Neglecting charge fluctuations and assuming a uniform charge deposit, the coefficients k_{11}, k_{12}, k_{22} vanish. Assuming very large readout pixels, the coefficients c_{11}, c_{12}, c_{22} vanish and k_{11}, k_{12}, k_{22} become $4/180, -7/180, 4/180$ in accordance with the above. For very small pixels, we have $k_{11} = 1/12$ and all other coefficients vanish, which is in accordance with an arrival time distribution of charges at the pad. Landau fluctuations and weighting field fluctuations are strongly correlated, so they cannot be decoupled or 'added in squares'. Since $k_{11} > k_{22}$, the effect of weighting field fluctuations is smallest if T_1 is small i.e. if the electrons move towards the readout pixel. In this case it seems possible that for values of $w/d \gtrsim 1$ the weighting field effect does not add significantly to the c.o.g. time resolution. We note that this calculation assumes perpendicular tracks and neglects diffusion.

- The expressions for leading edge discrimination of the normalized silicon sensor signal (i.e. the signal divided by the total charge) show that the c.o.g. time resolution is indeed recovered for large peaking times, and that for faster electronics the time resolution is significantly improved when placing the threshold at $< 40\%$ of the total signal charge. As an example, for a $50\,\mu$m sensor at 200 V, a peaking time of 1 ns and a threshold at 30 % of the normalized signal, the time resolution is 15 ps and the noise must be less than 70 electrons in order to not significantly add to this value. For a given series noise resistance e_n of an amplifier, the equivalent noise charge decreases with $1/\sqrt{t_p}$, the effect of the noise on time resolution does however increase linearly with t_p. It is therefore advantageous to use faster electronics if power consumption allows and other noise sources do not start to become dominant.

- The effect of the finite pixel size on the leading edge discrimination of the normalized signal can be calculated with the formulas given in this report, the numerical evaluation is however quite involved and a Monte Carlo simulation might be more efficient.

- For silicon sensors with gain (LGAD), the standard deviation of the c.o.g. time becomes

$$\Delta_\tau = \frac{1}{\sqrt{1+1.155\log d/\lambda}}\frac{T_1}{\sqrt{12}} \tag{112}$$

  This formula assumes that only the gain holes contribute to the signal. This expression is the same as the one for the very small pixels without gain and represents in essence an arrival time distribution. This resolution is significantly worse than the time resolution for a sensor without gain e.g. it evaluates to 60 ps for a $50\,\mu$m sensor at 200 V. The c.o.g. time is therefore not a good way to extract the time information for sensors with gain. Leading edge discrimination of the normalized signal is also not providing an improved time resolution, since the total charge of the sensor signal has no correlation to the arrival time of the first electrons. Fast electronics with leading edge discrimination as well as slewing corrections related to the slope of the leading edge, like double threshold or constant fraction discrimination, are therefore key to extract the best possible time information from this type of sensor.

- Including the effect of the finite pixel size on the c.o.g. time resolution of a silicon sensor with gain we find

$$\Delta_\tau = \sqrt{\frac{1}{1+1.155\log d/\lambda}\frac{T_1^2}{12} + s_{22}T_2^2} \tag{113}$$

  In contrast to sensors without gain there is no correlation between the Landau fluctuations and the weighting field fluctuations. For uniform charge deposit, only the second term of the expression remains. For very large and very small pads the coefficient s_{22} vanishes and the effect is largest for $w/d \approx 3$. In addition the expression is the same, whether the pixel is on the gain side or the opposite side of the sensor.

The solutions shown in this report set the scale of the problem and provide insight into some principle dependencies of the time resolution on charge fluctuations, noise and weighting field fluctuations. The inclusion of realistic charge deposit models as well as the effect of diffusion, track angle, finite depletion voltage and pixelization are best accomplished through Monte Carlo simulations and the formulas of this report can be used as benchmarks for such studies.

13. Appendix

The expression for the weighting potential of a rectangular pad of dimension w_x, w_y centred at $x = y = 0$ with a parallel plate separation of d is given in [25] as

$$\phi_w(x,y,z,w_x,w_y,d) = \frac{1}{2\pi} f(x,y,z,w_x,w_y) - \frac{1}{2\pi}\sum_{n=1}^{\infty}[f(x,y,2nd-z,w_x,w_y) - f(x,y,2nd+z,w_x,w_y)] \tag{114}$$

$$\begin{aligned} f(x,y,u,w_x,w_y) &= \arctan\left(\frac{x_1 y_1}{u\sqrt{x_1^2+y_1^2+u^2}}\right) + \arctan\left(\frac{x_2 y_2}{u\sqrt{x_2^2+y_2^2+u^2}}\right) && (115) \\ &- \arctan\left(\frac{x_1 y_2}{u\sqrt{x_1^2+y_2^2+u^2}}\right) - \arctan\left(\frac{x_2 y_1}{u\sqrt{x_2^2+y_1^2+u^2}}\right) && (116) \end{aligned}$$

$$x_1 = x - \frac{w_x}{2} \qquad x_2 = x + \frac{w_x}{2} \qquad y_1 = y - \frac{w_y}{2} \qquad y_2 = y + \frac{w_y}{2} \tag{117}$$

We note that

$$\phi_w(x,y,z,w_x,w_y,d) = \phi_w\left(\frac{x}{d},\frac{y}{d},\frac{z}{d},\frac{w_x}{d},\frac{w_y}{d},1\right) \tag{118}$$

The weighting field is given by

$$E_w^z(x,y,z,w_x,w_y,d) = \frac{1}{2\pi} g(x,y,z,w_x,w_y) + \frac{1}{2\pi}\sum_{n=1}^{\infty}[g(x,y,2nd+z,w_x,w_y) + g(x,y,2nd-z,w_x,w_y)] \tag{119}$$

with

$$\begin{aligned} g(x,y,u,w_x,w_y) &= \frac{x_1 y_1 (x_1^2+y_1^2+2u^2)}{(x_1^2+u^2)(y_1^2+u^2)\sqrt{x_1^2+y_1^2+u^2}} + \frac{x_2 y_2 (x_2^2+y_2^2+2u^2)}{(x_2^2+u^2)(y_2^2+u^2)\sqrt{x_2^2+y_2^2+u^2}} \\ &- \frac{x_1 y_2 (x_1^2+y_2^2+2u^2)}{(x_1^2+u^2)(y_2^2+u^2)\sqrt{x_1^2+y_2^2+u^2}} - \frac{x_2 y_1 (x_2^2+y_1^2+2u^2)}{(x_2^2+u^2)(y_1^2+u^2)\sqrt{x_2^2+y_1^2+u^2}} \end{aligned} \tag{120}$$

and it holds that

$$E_w^z(x,y,z,w_x,w_y,d) = \frac{1}{d} E_w^z\left(\frac{x}{d},\frac{y}{d},\frac{z}{d},\frac{w_x}{d},\frac{w_y}{d},1\right) \tag{121}$$

w/d	c_{22}	c_{12}	c_{11}	$c_{11}+c_{12}+c_{22}$
0	0	0	0	0
0.01	6.13×10^{-12}	-2.88×10^{-9}	3.44×10^{-7}	3.41×10^{-7}
0.1	6.05×10^{-8}	-2.75×10^{-6}	3.18×10^{-5}	2.91×10^{-5}
0.2	9.28×10^{-7}	-2.06×10^{-5}	1.17×10^{-4}	9.68×10^{-5}
0.25	2.2×10^{-6}	-3.88×10^{-5}	1.74×10^{-4}	1.37×10^{-4}
0.5	2.77×10^{-5}	-2.44×10^{-4}	5.5×10^{-4}	3.33×10^{-4}
1.	2.1×10^{-4}	-1.04×10^{-3}	1.33×10^{-3}	4.99×10^{-4}
1.5	4.5×10^{-4}	-1.78×10^{-3}	1.81×10^{-3}	4.86×10^{-4}
2.	6.13×10^{-4}	-2.18×10^{-3}	$2.\times10^{-3}$	4.34×10^{-4}
3.	7.13×10^{-4}	-2.31×10^{-3}	1.94×10^{-3}	3.41×10^{-4}
4.	6.83×10^{-4}	-2.14×10^{-3}	1.74×10^{-3}	2.77×10^{-4}
5.	6.26×10^{-4}	-1.93×10^{-3}	1.54×10^{-3}	2.32×10^{-4}
10	$4.\times10^{-4}$	-1.2×10^{-3}	9.27×10^{-4}	1.27×10^{-4}
20	2.24×10^{-4}	-6.64×10^{-4}	5.06×10^{-4}	6.61×10^{-5}
50	9.56×10^{-5}	-2.82×10^{-4}	2.13×10^{-4}	2.71×10^{-5}
∞	0	0	0	0

Table 1: Coefficients c_{11}, c_{12}, c_{22} from Eq. 68 for different vales of w/d, where w is the size of the square pixel and d is the thickness of the sensor.

w/d	k_{22}	k_{12}	k_{11}	$k_{11}+k_{12}+k_{22}$
0	0	0	$\frac{1}{12}=8.33\times10^{-2}$	$\frac{1}{12}=8.33\times10^{-2}$
0.01	8.43×10^{-8}	-6.43×10^{-5}	8.33×10^{-2}	8.32×10^{-2}
0.1	5.37×10^{-5}	-2.82×10^{-3}	8.05×10^{-2}	7.77×10^{-2}
0.2	3.05×10^{-4}	-7.32×10^{-3}	7.57×10^{-2}	6.87×10^{-2}
0.25	5.13×10^{-4}	-9.62×10^{-3}	7.32×10^{-2}	6.41×10^{-2}
0.5	2.17×10^{-3}	-1.94×10^{-2}	6.18×10^{-2}	4.46×10^{-2}
1.	6.39×10^{-3}	-2.96×10^{-2}	4.73×10^{-2}	2.41×10^{-2}
1.5	9.82×10^{-3}	-3.36×10^{-2}	3.99×10^{-2}	1.62×10^{-2}
2.	1.22×10^{-2}	-3.53×10^{-2}	3.58×10^{-2}	1.28×10^{-2}
3.	1.51×10^{-2}	-3.67×10^{-2}	3.15×10^{-2}	9.86×10^{-3}
4.	1.68×10^{-2}	-3.74×10^{-2}	2.92×10^{-2}	8.61×10^{-3}
5.	1.78×10^{-2}	-3.77×10^{-2}	2.78×10^{-2}	7.92×10^{-3}
10	$2.\times10^{-2}$	-3.83×10^{-2}	2.5×10^{-2}	6.68×10^{-3}
20	2.12×10^{-2}	-3.86×10^{-2}	2.35×10^{-2}	6.19×10^{-3}
50	2.29×10^{-2}	-3.84×10^{-2}	2.2×10^{-2}	6.44×10^{-3}
∞	$\frac{4}{180}=2.2\times10^{-2}$	$-\frac{7}{180}=-3.89\times10^{-2}$	$\frac{4}{180}=2.2\times10^{-2}$	$\frac{1}{180}=5.56\times10^{-3}$

Table 2: Coefficients k_{11}, k_{12}, k_{22} from Eq. 77 for different vales of w/d, where w is the size of the square pixel and d is the thickness of the sensor.

References

[1] G. Aglieri Rinella et al., The NA62 Gigatracker *Nucl. Instrum. Meth. Phys. Res., Sect. A* 845 (2017), 147-149.

[2] G. Aglieri Rinella et al., The TDCpix readout asic: A 75 ps resolution timing front-end for the Gigatracker of the NA62 experiment. Proceedings of the 2nd International Conference on Technology and Instrumentation in Particle Physics (TIPP 2011). *Physics Procedia*, 37 (2012), 1608-1617.

[3] A. Kluge et al., The TDCpix readout asic: A 75 ps resolution timing front-end for the NA62 Gigatracker hybrid pixel detector. *Nucl. Instrum. Meth. Phys. Res., Sect. A* 732 (2013), 511-514.

[4] M. Fiorini et al., High rate particle tracking and ultra-fast timing with a thin hybrid silicon pixel detector. *Nucl. Instrum. Meth. Phys. Res., Sect. A* 718 (2013), 270-273.

[5] M. Benoit et al., 100ps time resolution with thin silicon pixel detectors and a SiGe HBT amplifier, 2016 JINST 11 P03011

[6] G. Pellegrini et al., Technology developments and first measurements of Low Gain Avalanche Detectors (LGAD) for high energy physics applications. *Nucl. Instrum. Meth. Phys. Res., Sect. A* 765 (2014), 12-16.

[7] N. Cartiglia et al., Performance of ultra-fast silicon detectors. *J. Instr.*, 9(2), 2014.

[8] H.F.-W. Sadrozinski et al., Ultra-fast silicon detectors. *Nucl. Instrum. Meth. Phys. Res., Sect. A* 730 (2013), 226-231.

[9] H.F.-W. Sadrozinski et al., Sensors for ultra-fast silicon detectors. *Nucl. Instrum. Meth. Phys. Res., Sect. A* 765 (2014), 7-11.

[10] N. Cartiglia et al., Design optimization of ultra-fast silicon detectors. *Nucl. Instrum. Meth. Phys. Res., Sect. A* 796 (2015), 141-148.

[11] N. Cartiglia et al., Beam test results of a 16 ps timing system based on ultra-fast silicon detectors. *Nucl. Instrum. Meth. Phys. Res., Sect. A* 850 (2017), 83-88.

[12] F. Cenna et al., Weightfield2: A fast simulator for silicon and diamond solid state detector. *Nucl. Instrum. Meth. Phys. Res., Sect. A* 796 (2015), 149-153.

[13] N. Cartiglia et al., Tracking in 4 dimensions. *Nucl. Instrum. Meth. Phys. Res., Sect. A* 845 (2017), 47-51.

[14] V. Sola et al., Ultra-fast silicon detectors for 4D tracking. *J. Instr.*, 12(02):C02072, 2017.

[15] S. Parker et al., Increased speed: 3D silicon sensors; fast current amplifiers. *IEEE Trans. Nucl. Sci.*, 58(2):404–417, April 2011.

[16] H. Spieler, Fast timing methods for semiconductor detectors. *IEEE Trans. Nucl. Sci.*, 29(3):1142–1158, June 1982.

[17] A. Rivetti, Fast front-end electronics for semiconductor tracking detectors: Trends and perspectives. *Nucl. Instrum. Meth. Phys. Res., Sect. A* 765 (2014), 202-208.

[18] J.H. Jungmann and R.M.A. Heeren, Emerging technologies in mass spectrometry imaging. *Journal of Proteomics*, 75(16):5077-5092, 2012.

[19] C. Vallance et al., Fast sensors for time-of-flight imaging applications. *Physical Chemistry Chemical Physics*, 16(2):383–395, 2014.

[20] H. Schindler, Microscopic simulation of particle detectors, CERN-THESIS-2012-208, https://cds.cern.ch/record/1500583/

[21] W. W. M. Allison and J. H. Cobb, Relativistic charged particle identification by energy loss, Ann. Rev. Nucl. Part. Sci. 30 (1980), 253-298

[22] K. Nakamura et al. (Particle Data Group), The Review of Particle Physics J. Phys. G37, 075021 (2010)

[23] Synopsis, Inc., Sentaurus Device User Guide Version D-2010.03.

[24] W.E. Cleland, E.g. Stern, Signal processing considerations for liquid ionization calorimeters in a high rate environment, *Nucl. Instrum. Meth. Phys. Res., Sect. A* 338 (1994) 467-497

[25] W. Riegler and G. Aglieri Rinella, Point charge potential and weighting field of a pixel or pad in a plane condenser. *Nucl. Instrum. Meth. Phys. Res., Sect. A* 767 (2014), 267-270.

[26] C. Canali et al., *IEEE Trans. Electron Dev.* 22, 1045 (1975)